TAMPEREEN TEKNILLINEN YLIOPISTO
TAMPERE UNIVERSITY OF TECHNOLOGY

ADNAN HANIF

MEASUREMENT OF CORE LOSSES IN TOROIDAL INDUCTORS WITH DIFFERENT MAGNETIC MATERIALS

Master of Science thesis

Examiners: Assist. Prof. Paavo Rasilo and
Assoc. Prof. Elena Simona Lohan
Examiner and topic approved by the Council of the Faculty of Commuting and Electrical Engineering on 29th Mar 2017

ABSTRACT

ADNAN HANIF: Measurement of core losses in toroidal inductors with different magnetic materials
Tampere University of technology
Master of Science Thesis, 54 pages,
June 2017
Master's Degree Programme in Electrical Engineering Technology
Major: Wireless Communication Circuits and Systems
Examiners: Assist. Prof. Paavo Rasilo, Assoc. Prof. Elena Simona Lohan

Keywords: core loss, hysteresis loop, flux density, saturation flux, magnetization, toroidal cores, power loss density

Magnetic materials are used in the manufacturing of transformers, electrical machines, converters and inductors. The losses of the magnetic materials affect the performance of the electromagnetic devices. The magnetic components play an important role in dissipating the core losses in power electronics devices. Measuring the losses in the magnetic materials is necessary since this data can then be used to identify the eddy-current and hysteresis loss models.

The core loss is produced due to the realignment of magnetic domains and wall movements. The eddy currents are caused by the non-zero conductivity of material under an alternating external magnetic field. The eddy currents and hysteresis loss are the origin of core losses. The B-H loops measurement technique is the common approach for measuring the core losses. In this approach, two windings are used for the test core. The main benefit of this approach is that the measurements do not include the copper losses. Since the voltage is measured at the secondary winding, so the voltage drop across the resistance of the primary winding will not affect the measurement results.

This thesis investigated the core losses in soft magnetic materials, for example ferrite, molypermalloy powder (MPP), nanocrystalline and amorphous. The measurements were taken under the sinusoidal voltage excitation up to a frequency of 1 kHz. The effects of temperature were not considered in the core loss measurements, which may have influenced the measured results. A comparison of the core losses under different magnetic field density and frequencies is presented. The experimental data showed that nanocrstalline material has the lowest losses whereas amorphous has the highest core losses. The ferrite material has almost double the losses as compared to nanocrystalline. On the other hand, it has been noticed that MPP core shows some variation in the results due to the temperature rise in the core.

PREFACE

This master thesis is written as a part of completion of a Master of Science (Technology) degree in Electrical Engineering. The research work was completed at the department of Electrical Engineering in Tampere University of Technology under the supervision of Assistant Professor Mr. Paavo Rasilo.

I would like to express my heartiest gratitude to Paavo for his ideas, guidance and support during the entire research work. He helped me a lot throughout my thesis and I learnt many new things especially in electromagnetics. I would also like to thank Assoc. Prof. Elena Simona Lohan for her supportive supervision, who is the co-supervisor of this thesis from the department of Electronics and Communication Engineering.

I would like to thank my parents for their prayers and support throughout my life. Finally, I would like to thank my beloved wife for her endless moral support and encouragement.

Tampere, 24.5.2017

Adnan Hanif

CONTENTS

LIST OF SYMBOLS AND ABBREVIATIONS

ac	Alternating current
dc	Direct current
MPP	Molypermalloy powder
A_{c}	Cross-section area of the core
A_{e}	Effective area of the core
A_{s}	Surface area
A_{w}	Area of cross section of wire
A_{wp}	Area of cross section of primary wire
B, $\boldsymbol{B}$	Magnetic flux denity
B_{max}	Maximum flux density
B_{pk}	Peak magnetic flux density
B_{r}	Remanent flux
d_1	Bare wire diameter of primary wire
h	Height of toroidal core
H, $\boldsymbol{H}$	Magnetic flux density
H_{c}	Coercive force
H_{ext}	External field intensity
$I_{\mathrm{p\_rms}}$	Primary rms current
i_{E}	Eddy current
$i_{\mathrm{p}}(t)$	Exciting current
ID	Inner diameter of core
J	Current density
K_{e}	Eddy-current loss constant
K_{h}	Hysteresis loss constant
l	Total length of the magnetic path
l_{c}	Mean length of the magnetic core
l_{1turn}	Length one turn
$l_{\mathrm{p\_w}}$	Total length of primary wire
$l_{\mathrm{s\_w}}$	Total length of secondary wire
l_{w}	Total length of wire
L	Initial length of material
M_{r}	Remanent magnetization
N	Total number of turns
N_1	Number of primary turns
N_2	Number of secondary turns
OD	Outer diameter of core
p_{loss}	Core loss per unit volume
P_{c}	Total core loss
P_{cu}	Copper loss
$P_{\mathrm{Cu\_p}}$	Copper loss of primary wire
P_{e}	Eddy current loss
$P_{\mathrm{exc.}}$	Excess loss
P_{h}	Hysteresis power loss
P_{ρ}	Volt ampere per unit mass
R_{dc}	Dc resistance

$R_{\mathrm{p\_dc}}$	Dc resistance of primary wire
$v_{\mathrm{s}}(t)$	Sensing voltage
V_{core}	Volume of the core
$V_{\mathrm{s\_rms}}$	Secondary wire voltage
W_{cycle}	Energy loss over one cycle
W_{h}	Energy density in one cycle

Φ	Magnetic flux
λ	Flux linkage
μ	Magnetic permeability
μ_{o}	Permeability of free space
μ_{o}	Relative permeability of the material
ρ	Resistivity of the copper
δ	Skin effect
σ	Conductivity
ρ_{c}	Mass density of core
λ_{m}	Magnetostriction
λ_{s}	Saturation magnetostriction

1. INTRODUCTION

Magnetic materials are broadly utilized in the manufacturing of transformers, electrical machines, converters and inductors. A good understanding of materials is required for the selection of material and size. An inaccurate design can cause extra losses and undesirably influence the performance of the device [1].

The losses of the applied soft-magnetic materials affect the performance of the electromagnetic devices. By increasing the operation frequency, high power densities can be accomplished but higher frequency produces higher loss density. At higher frequencies, nanocrystalline and amorphous materials take advantage from reduced losses caused by the eddy currents. The iron losses in soft-magnetic materials depend on many factors for example, operational frequency and the material specifications. The traditional materials for instance silicon steel are used in the applications with an operational frequency less than 1 kHz. The addition of nanocrystalline and amorphous materials allowed new ways to design electromagnetic circuits [2].

For industrial goals, the advancement in the soft magnetic materials began with laminated iron and carries on with carbonyl iron, powdered, ferrite, the latest nanocrystalline materials and amorphous materials. The required properties of the magnetic material vary with the applications. High saturation flux density, high permeability, low power loss and low coercivity are desirable in most of the applications of soft magnetic materials. Moreover, the mechanical properties of the materials are also essential. Generally, in a single material it is possible to have all the required properties. Therefore, the decision of the material is typically a bargain for a given application [3].

1.1 The aim and scope

The core loss is produced due to the realignment of magnetic domains and wall movement. A magnetic domain contains a uniform magnetization. When the domain walls move under an alternating external magnetic field, energy is absorbed which turns into core loss. Eddy current loss and hysteresis loss are the origin of core losses. The energy absorbed to change the direction of the magnetic moments is called hysteresis loss. It represents the area enclosed by the static hysteresis loop.

The relation between magnetic field intensity H and flux density B is depicted by the B-H loop of a magnetic material. Due to the iron losses, the B-H curve becomes a hysteresis loop and the area of the loop denotes energy losses [4]. Many kinds of electronics devices, electric machines, magnetic recording, and permanent magnets massively depend on the

aspects of hysteresis. The aim of this thesis to measure the hysteresis losses of soft magnetic materials for example ferrite, molypermalloy powder (MPP), nanocrystalline and amorphous up to a frequency of 1 kHz. This data can then be used to identify hysteresis and eddy current loss models. The measurement method described in [4] and [5] are applied to measure the hysteresis losses and B-H loops.

1.2 The outline

The background theory regarding magnetic fundamentals and core losses is presented in Chapter 2. The properties and structure of ferromagnetic materials are explained in Chapter 3. The characteristics of the investigated materials used in this thesis are explained in Chapter 4. The toroidal core design is explained in Chapter 5. The measurement method and working principle of measuring for B-H loop and core loss are explained in Chapter 6. The results obtained by the proposed method and possible problems observed during measurements are discussed in Chapter 7. In the end, the conclusion of the entire work is written in Chapter 8.

2. MAGNETIC THEORY FUNDAMENTALS

2.1 Magnetic and electrical relationships

A magnetomotance (mmf) is produced when an inductor of N turns carries a current as shown in Figure 2.1. The mmf acts as a source and it drives the magnetic circuit [6]. The Ampere's law defines that the line integral of the magnetic field intensity H around any closed loop is equal to the total current passing through the interior of the loop. The Ampere's law can be written as

$$\oint_l \boldsymbol{H} \cdot d\boldsymbol{l} = \int_s \boldsymbol{J} \cdot d\boldsymbol{S} = Ni \tag{2.1}$$

where H is the magnetic field intensity, J is the current density and N is the total number of turns of the coil each carrying a current i.

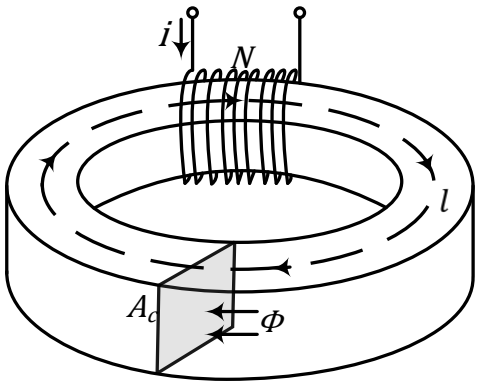

Figure 2.1: *Toroidal core with windings*

For a uniform magnetic field and parallel to path l, the mmf is expressed as

$$mmf = Ni = Hl \tag{2.2}$$

where l represents the mean magnetic path length of the core. The product of the total number of turns N, and the current i gives the amperes turns. The magnetic flux Φ is compelled to flow in a magnetic circuit by the mmf [7]. The total magnetic flux Φ passing through a surface S is given as

$$\Phi = \int_s \boldsymbol{B} \cdot d\boldsymbol{S} \tag{2.3}$$

When the magnetic flux density B is constant and perpendicular to the whole surface area A_c, then the magnetic flux Φ passing through that surface is given by

$$\Phi = BA_c \tag{2.4}$$

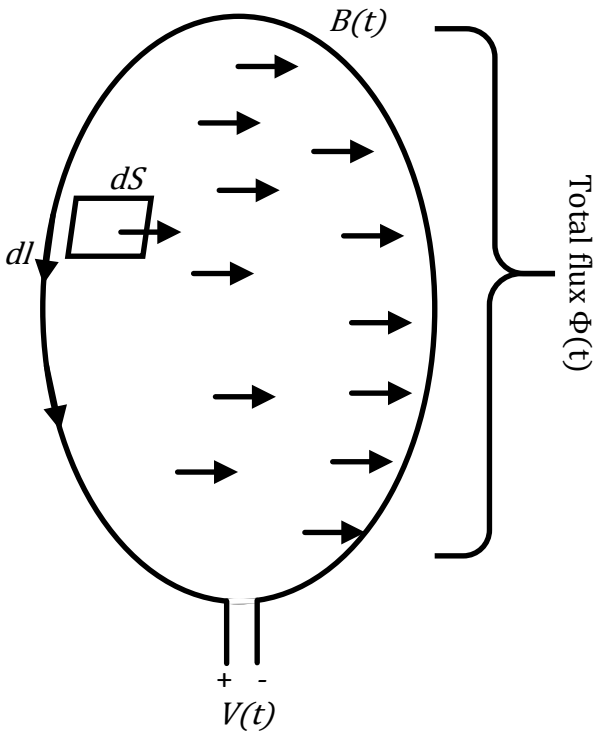

Figure 2.2: *Illustration of Faraday's law.*

The illustration of Faraday's law can be seen in the Figure 2.2 and it says that the line integral of the electric field intensity E around a closed path is equal to the time rate of change of the magnetic flux passing through the close path. When a time varying magnetic flux $\Phi(t)$ passes through a closed loop, it produces voltage in that loop [3], [8]. The relationship between the magnetic flux $\Phi(t)$ and the produced voltage $v(t)$ can be expressed as

$$v = -N\frac{d\Phi}{dt} \tag{2.5}$$

As long as the flux is changing voltage will be induced in the circuit. Moreover, the amount of the induced voltage is equal to the time rate of change of flux linkage in the

circuit [9]. According to Faraday's law, if the winding resistance is negligible then the average flux density through the coil is

$$B = \frac{1}{NA_c} \int vdt \tag{2.6}$$

where v is the terminal voltage of the coil and A_c is the area of cross section of the core. The total amount of flux surrounded by each turn of the coil is called magnetic flux linkage [1]. For a coil of the length l and cross sectional area A_c the flux linkage is written as

$$\lambda = N\Phi = \mathrm{N}A_c B = \mathrm{N}A_c \mu H = \frac{N^2 A_c \mu i}{l} \tag{2.7}$$

Lenz's law says that a rapidly changing magnetic flux $\Phi_a(t)$ generates a voltage. The direction of the voltage is such that it produces a current $i_E\,(t)$ in the closed loop.

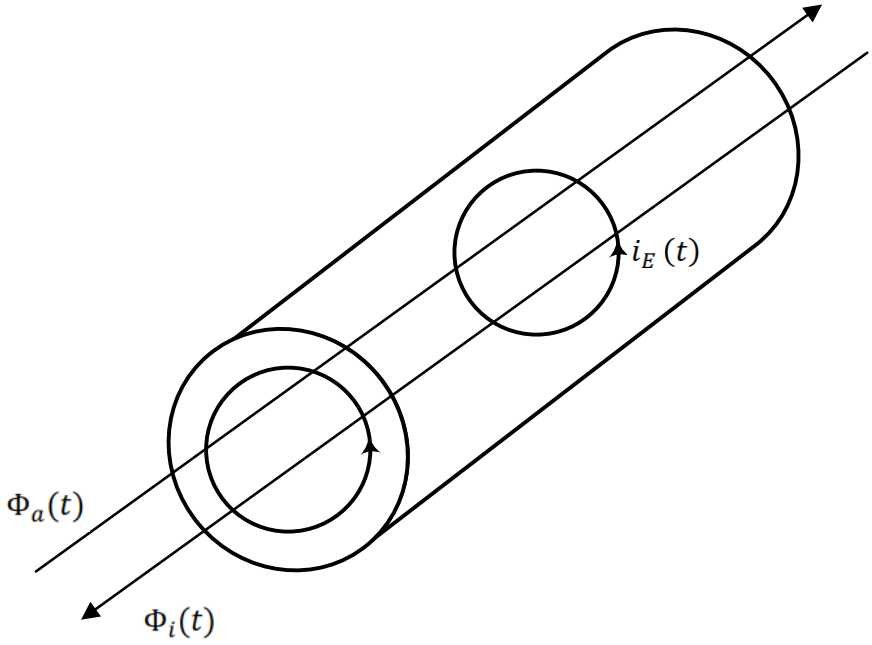

Figure 2.3: *Interpretation of Lenz's law*

The current induces a flux $\Phi_i(t)$ that prevents the change in the applied flux [3]. Figure 2.3 is showing induced currents caused by the varying magnetic field. Eddy currents produce non-uniform current distribution in the magnetic cores and coil conductors. This phenomena produces higher power losses, higher effective resistance and lower internal inductance [6].

According to Gauss's law of magnetic circuit, for any closed surface S the total flux going into the volume is precisely equivalent to the total flux going out of the volume [3]. The resulting flux through the surface is given by

$$\int_s \boldsymbol{B} \cdot d\boldsymbol{S} = 0 \tag{2.8}$$

2.2 Magnetic permeability

The relationship between the magnetic field intensity H and the magnetic flux density B can be established by defining the magnetic permeability as follows

$$B = \mu_o \mu_r H = \mu H \tag{2.9}$$

where μ is the permeability, μ_o represents the permeability of free space, and μ_r denotes the relative permeability of the material. The permeability is the ability that a material has to conduct flux. The magnitude of the permeability tells how a core material can be magnetized at a given induction [7]. A small field strength H produces a large magnetic flux density B at high value of μ_r. The magnetic flux Φ follows the path of highest permeability [6]. On a macro scale, we can imagine that the magnetic field intensity H is produced by electric current and magnetic field intensity B is the result of driving force H [9]. The maximum operating magnetic flux density B_m should be smaller than the saturation flux density B_{sat} of the core material [6].

2.3 The hysteresis loop (B-H loop)

A complete cycle of magnetization and demagnetization of a magnetic material under alternating sinusoidal operation is presented in Figure 2.4. The B-H loop shows the relationship between magnetic flux density B versus magnetic field intensity H. The maximum attainable magnetic flux density of the material is confined because of magnetic saturation. The hysteresis loss and magnetic flux saturation make the B-H curve nonlinear [4].

The dotted line denotes an idealized magnetization curve. It shows that the magnetic material is completely demagnetized and magnetic field strength H gradually rises until saturation point B_{sat} is reached. At this saturation point, the applied external field aligned the domains of the core along its direction. The B-H loop shifts its path to B_r as H drops. Even the H approaches to zero, the core still magnetized. At this point, the flux is called remanent flux B_r. When the magnetic field strength H further reduces, the point where magnetic flux density becomes zero, is called the coercive magnetic field H_c. The negative magnetizing force is required to demagnetize the core completely.

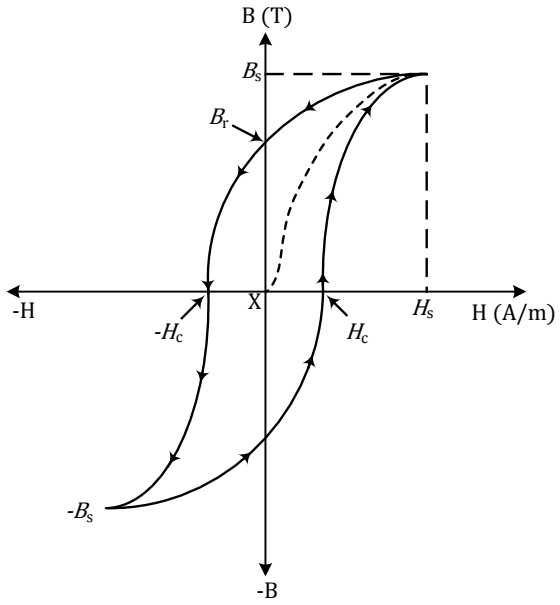

Figure 2.4: *Typical hysteresis loop illustration.*

If the magnetizing force is increased in the reverse direction, saturation in the opposite direction is similarly obtained. The loop completes its cycle according to the frequency of operation, and it has corresponding points on the opposite side as well. The area surrounded by the loop demonstrates the energy lost in the core material per hysteresis loop and this loop is called B-H loop or hysteresis loop. This process repeats continuously in ac applications and total hysteresis power loss depends on frequency [7].

2.4 Magnetic losses

The losses in the magnetic components can be characterized as core loss and winding loss. The winding loss is copper loss of the wire and core loss consists of hysteresis loss and eddy current loss. A changing magnetic field in the core produces losses in the core material. There are three types of core losses hysteresis, eddy current and anomalous loss. The hysteresis of the material makes the hysteresis loss a static loss while the other two dynamic losses are yielded by the eddy currents in the material. The classical eddy current loss originates in the material when a changing magnetic field is applied. This classical eddy current loss is also called the macroscopic eddy current loss. Whereas anomalous loss sometimes is called microscopic eddy current loss, which is generated by domain wall motion [10].

2.4.1 Hysteresis loss

When an ac field is applied to the magnetic material, the magnetic field intensity leads the magnetic flux density during the whole cycle of magnetization and demagnetization.

During each cycle, the area enclosed by the loop represents an amount of energy absorbed in the core. This absorbed energy gives rise to core heating and this loss of power is called hysteresis loss [7]. Figure 2.5 shows a uniformly wound insulated coil on a toroidal core. The coil has no resistance and the flux in the core is Φ.

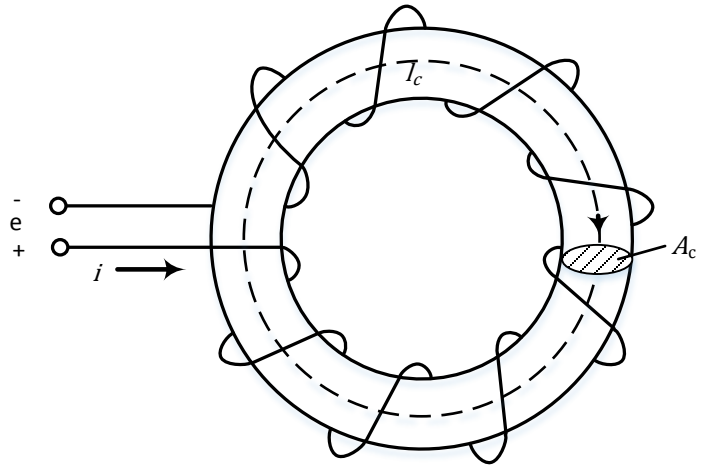

Figure 2.5: *Circuit diagram to measure hysteresis loss.*

The internal molecular resistance repels the constant realignment of domains in ferromagnetic materials. When the material completes its magnetization phase, the energy is also released in the form of heat [9]. According to Faraday's law, the applied voltage v is $v = N\frac{d\Phi}{dt}$. The energy loss W_{cycle} over one complete cycle of the hysteresis loop in the core can be written as

$$W_{\text{cycle}} = V_{\text{core}} \oint HdB \tag{2.10}$$

$$W_{\text{cycle}} = V_{\text{core}} W_{\text{h}} \tag{2.11}$$

where V_{core} represents the magnetic core volume, and $W_{\text{h}} = \oint HdB$ is the energy density in one full cycle [11]. The hysteresis effect produces the power loss and it can be stated as

$$P_{\text{h}} = V_{\text{core}} W_{\text{h}} f \tag{2.12}$$

where f is the frequency of the flux density. According to Charles Steinmetz, the approximate relation to the hysteresis loss can be expressed as

$$P_{\mathrm{h}} = K_h B_{\mathrm{max}}^{\mathrm{n}} f \tag{2.13}$$

where B_{max} is the maximum flux density, K_{h} is a constant and the value of n is between 1.5 to 2.5. The value of K_{h} depends on the volume of the core and type of the core material.

2.4.2 Copper loss and eddy current loss

Due to the high conductivity of the copper, most of the windings of the inductors are constructed using copper. Its high flexibility reduces the total volume and amount of copper required for the windings because copper has the ability to fit into compact windings around a magnetic core. Although the copper has a high conductivity, yet the electrical loss is a vital cause of heat at current densities used in inductors. The heat is the source of temperature rise in both of the magnetic core and windings [12]. In Figure 2.6, an equivalent circuit of a winding is shown.

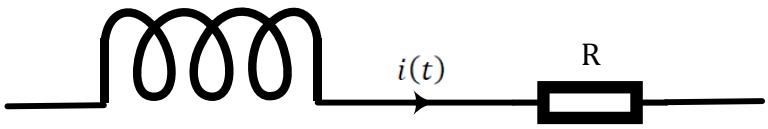

Figure 2.6: *Equivalent circuit model of winding for copper loss*

The winding of an inductor consists of wire of resistance R. It produces heat in the form of I^2R loss. The copper loss of the winding can be expressed as

$$P_{\mathrm{cu}} = I_{\mathrm{rms}}^2 R_{\mathrm{dc}} \tag{2.14}$$

where 'I_{rms}' denotes the rms current. The dc resistance of the winding of the inductor is written as

$$R_{\mathrm{dc}} = \rho \frac{l_{\mathrm{w}}}{A_{\mathrm{w}}} \tag{2.15}$$

where l_{w} is the total length of the wire, ρ is the resistivity of the copper and A_{w} is the wire bare cross sectional area [13].

The winding resistance increases with the frequency of the applied current. The growth in the resistance is because of the proximity effect and skin effect that limits the effective area of the copper cross section. The conductors are usually close to each other. When an alternating current flows through a conductor, it creates magnetic fields that induce the

adjacent conductors will give rise to an additional non-uniform distribution of the current density. The two adjacent conductors with current flowing in the same direction are shown in Figure 2.7 and in the opposite direction are shown in Figure 2.8.

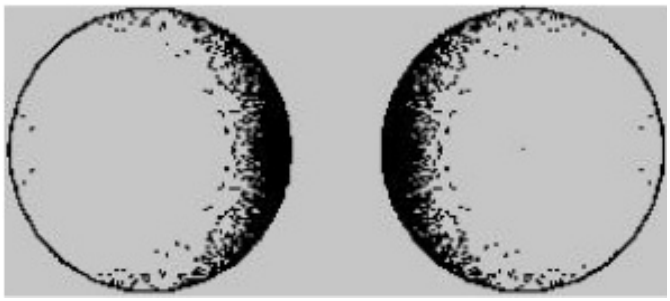

Figure 2.7: *Proximity effect with current flow in same direction* [14].

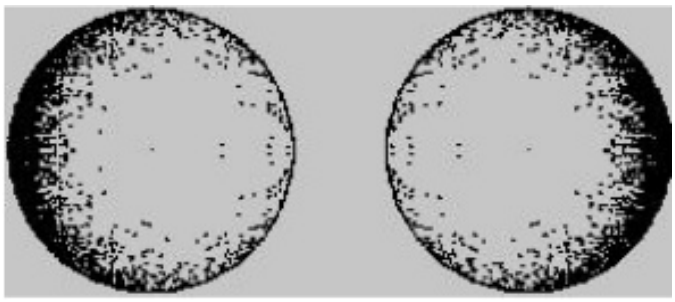

Figure 2.8: *Proximity effect with current flow in opposite direction* [14].

Two neighboring conductors with currents in a similar direction will have the maximum current density in the part next to the neighboring conductor. If the direction of current in one conductor changes then the current density will collect in the part uttermost far from the other conductor.

The copper loss is prone to the skin effect at higher frequencies [9]. The skin effect defines the non-uniform current density in the single conductor and give rise to increase the loss in inductors. The eddy currents will oppose the ac flux and as a result, the effective resistance of the conductor increases and reduces the net area available for current flow. The skin depth is expressed by

$$\delta = \frac{1}{\sqrt{\pi f \mu \sigma}} \tag{2.16}$$

where f denotes the frequency, σ is the conductivity and μ is the magnetic permeability of the conductor. Skin effect does not have too much effect at lower frequencies but it is more ambiguous at higher frequencies [12]. A large portion of the current is constrained within one skin depth of the surface, so that the conduction area reduces as the frequency rises. Because of the skin effect, the alternating current produces higher resistance in metallic conductors compared with direct current and hence higher power loss [9].

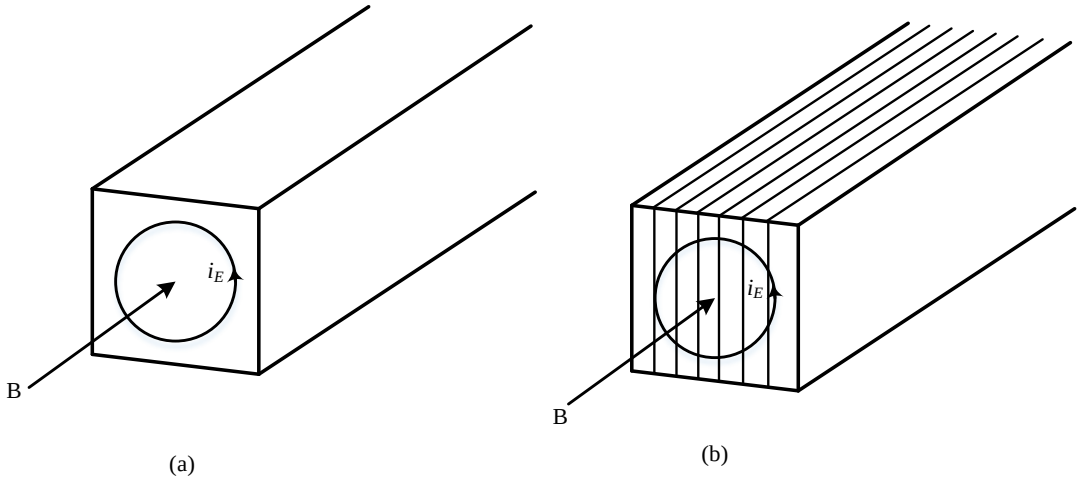

Figure 2.9: *Interpretation of eddy current in a magnetic core: (a) Solid core. (b) Laminated core.*

The rapid change in the flux density B through the cross section of a core is presented in Figure 2.9. If flux density fluctuates swiftly in the core, the loss of power takes place. The fast change of flux density in the cross section of the core is shown in the Fig. 1.7 a. As a result of changing magnetic flux in the enclosed path, a voltage is induced in the path of the cross-section. Therefore, a current i_{E} runs around the path [11]. Due to the resistance of the core material, this eddy current i_E generates I^2R loss in the core and heat flows out of the core. The eddy current loss is dependent on the time-varying magnetic flux and is written as

$$P_{\mathrm{e}} = K_{\mathrm{e}} B_{\mathrm{max}}^2 f^2 \tag{2.17}$$

where K_{e} is a constant and its value relies on lamination thickness and magnetic material [11]. Bertotti proposed the excess or anomalous loss in [15] is given as $P_{\mathrm{exc.}} = K_{\mathrm{exc.}} B_{\mathrm{max}}^{1.5} f^{1.5}$, where $K_{exc.}$ is the excess coefficient. The total core loss contains the eddy current loss, hysteresis loss and anomalous loss given as

$$P_{\mathrm{c}} = P_{\mathrm{h}} + P_{\mathrm{e}} + P_{\mathrm{exc.}} \tag{2.18}$$

2.5 AC excitation in the magnetic core

Figure 2.10 is showing a toroidal core, where primary and secondary windings are wound on the magnetic core. The mean magnetic path length of the core is l_c and the cross sectional area of the core is A_c. A sinusoidal voltage is applied to the primary winding and the secondary winding is in open-circuit under no load conditions.

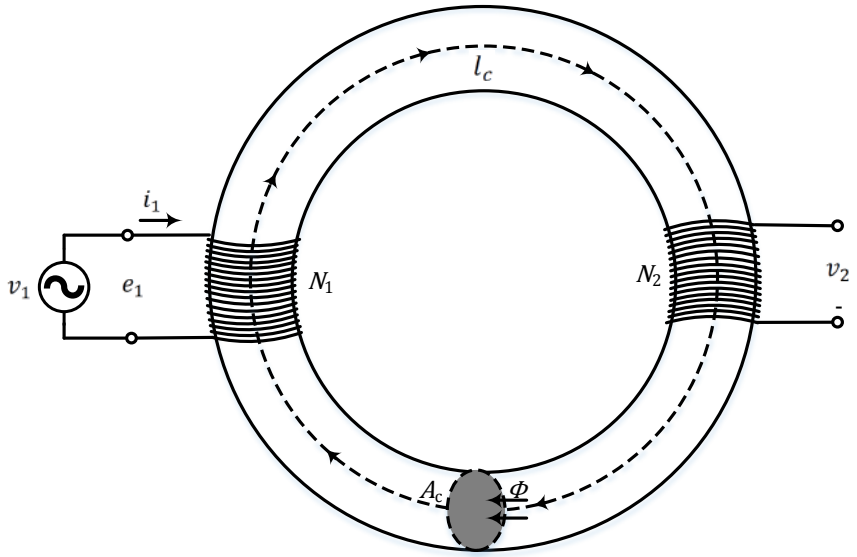

Figure 2.10: *Toroidal core with primary and secondary windings without load*

According to the Ampere's law and Faraday's law, the induced emf in the primary side is given as

$$e_1 = N_1 \frac{d\Phi_1}{dt} \tag{2.19}$$

The primary winding has a resistance R_1, so some voltage will drop in the primary windings. The primary voltage together with voltage drop in primary windings of resistance R_1 is given as

$$v_1 = R_1 i_1 + e_1 \tag{2.20}$$

A magnetizing current i_1 in the primary winding produces a time varying flux Φ in the core. The instantaneous flux $\Phi(t)$ can be written as

$$\Phi(t) = \Phi_{max}\, sin\omega t = A_c B_{max} sin\omega t \tag{2.21}$$

where $\Phi_{\max}$ is the amplitude of the core flux, $B_{\max}$is the amplitude of the flux density and $\omega = 2\pi f$ is the angular frequency. Then (2.21) becomes

$$e_1 = \omega N_1 A_c B_{\max} cos\omega t \tag{2.22}$$

The amplitude of the induced emf in primary is

$$E_{1\max} = 2\pi f N_1 A_c B_{\max} \tag{2.23}$$

The rms value of the induced emf in primary is

$$E_{1\text{rms}} = \frac{E_{1\max}}{\sqrt{2}} = 4.44 f N_1 A_c B_{\max} \tag{2.24}$$

If we neglect the resistance, then $E_{1\text{rms}} = V_{1\text{rms}}$. Then rms value of input voltage for sinusoidal excitation is given by

$$V_{1\text{rms}} = 4.44 f N_1 A_c B_{\max} \tag{2.25}$$

The exciting current i_1 in the primary winding is needed in order to produce magnetic flux in the core. Due to the nonlinear property of the magnetic core, the waveforms of sinusoidal flux and current vary from each other [8]. According to (2.2), the exciting current in the primary winding is

$$i_1 = \frac{H l_c}{N_1} \tag{2.26}$$

The rms value of exciting current in the primary winding can be written as

$$I_{1\text{rms}} = \frac{H_{\text{rms}} l_c}{N_1} \tag{2.27}$$

The rms volt-amperes needed to excite the core is expressed as

$$V_{1\text{rms}} I_{1\text{rms}} = 4.44 f B_{\max} H_{\text{rms}} A_c l_c \tag{2.28}$$

The rms volt-amperes per unit mass P_ρ for a magnetic material of mass density ρ_c is

$$P_\rho = \frac{V_{1\text{rms}} I_{1\text{rms}}}{mass} = \frac{4.44 f}{\rho_c} B_{\max} H_{\text{rms}} \tag{2.29}$$

where $A_c l_c$ is the volume of the core. The exciting current delivers the desired emf to generate the core flux and input power linked with energy in the core. Some part of this energy is released in the form of core heating. The remaining energy acts as reactive power associated with energy storage in the magnetic field. This reactive power does not deplete in the core. It is consumed by the excitation source [8].

3. MAGNETIC MATERIALS

In numerous engineering systems, magnetic materials play a vital role. The magnetic materials are categorized into three groups based on their magnetic properties. Those three groups are diamagnetic, paramagnetic and ferromagnetic materials. The susceptibility is small and negative for diamagnetic materials and it has a value of about -10^{-5}. Copper, silver and beryllium are the diamagnetic materials.

The magnetic response of diamagnetic materials resists the applied magnetic field. Aluminum, platinum and manganese fall into the category of paramagnetic materials due to their small and positive susceptibility. The value of relative susceptibility for this magnetic material group varies between 10^{-3} to 10^{-5}. Paramagnetic materials produce weak magnetization aligned with the external field. Ferromagnets are the most commonly known magnetic materials and their susceptibility can be varied typically between 50 and 10,000. Cobalt, nickel and iron are ferromagnetic materials [16].

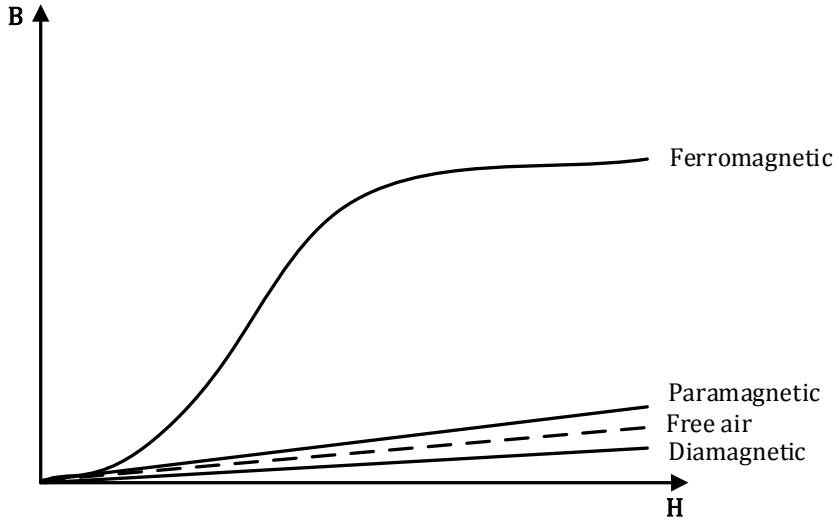

Figure 3.1: *The B-H curves for different kind of magnetic materials* [1]

The *B* and *H* relationship for the diamagnetic and paramagnetic materials is linear and their relative permeability μ_r is close to unity. Diamagnetic materials have a slight tendency to forbid the magnetic field, because of their μ_r value is less than unity. The permanent magnetic moments do not exist among the atoms of diamagnetic materials. Due to a value of μ_r bigger than unity, paramagnetic materials can be slightly magnetized with an external magnetic field [3]. Figure 3.1 is showing the B-H relation of different magnetic materials. In this thesis, the discussion is focused on ferromagnetic materials.

[1] [3]

3.1 Ferromagnetic material

Due to the high permeabilities of the ferromagnets, they are used in most of the engineering applications and high magnetic inductions can be achieved with simple magnetic fields. The initial relative permeabilities of ferromagnets are usually between 10 to 10^5. The ferromagnetic materials are often categorized based on their coercivity. Coercivity depends on the structure of the magnetic material, it can be changed by exposing the sample to disparate mechanical and thermal analysis, as for instance saturation magnetization cannot. The ferromagnets are classified into two main groups based on their coercivity, soft magnets and hard magnets. The value of coercivity for hard magnetic materials is more than 10 kA/m and for soft magnetic materials is less than 1 kA/m [16].

3.1.1 Structure of the material

Ferromagnetism relies on the characteristic of domains. The magnetic material contains these minute regions. The minute regions have this unique property that the atoms of the particular domain have their own specific spins arranged in the similar direction [17]. Each electron in an atom revolves around the nucleus and rotates around its own axis as well. The rotation of the electrically charged electron creates a magnetic moment [3].

Electrons are present in pairs in most of the atoms and they spin in the opposite way. The opposite spins of paired electrons force their magnetic moments to wipe out each other and hence no net magnetic moment occurs. On the other hand, the materials that have more unpaired electrons will have non-zero net magnetic moment. There are unpaired electrons in ferromagnetic materials. Their atoms reveal a net magnetic moment and a magnetic dipole appears in each atom. The interaction occurs between the dipoles of two adjacent atoms when a ferromagnetic material experiences an external field and this external field lines up the dipoles in its direction. Due to the interactive act, amplification of the external field outcomes in high magnetization even if the applied field is weak. The dipoles interact with the adjacent dipoles even if there is no external field and this results in the parallel arrangement. The region where all the dipoles are arranged is known as the magnetic domain [18].

When both the atomic moments and crystal lattice sites are aligned parallel, then the ferromagnetic effect is produced due to the moments of each atom add up. The whole structure does not face this arrangement of atomic magnets apart from certain places in the structure [3]. The domain structure is changed by the application of an applied magnetic field. The domains can be arranged easily related to external field rise at the cost of those who are less favorably arranged resulting in the net magnetization does not stay at zero [17].

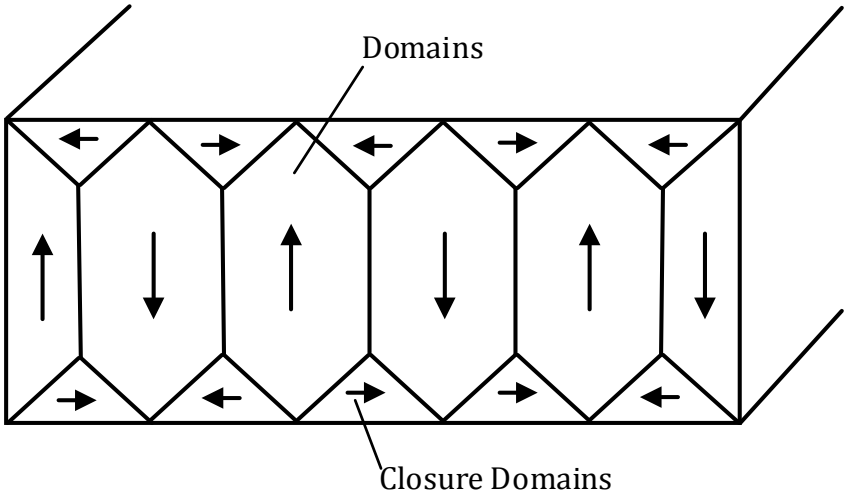

Figure 3.2: *Arrangement of magnetic domain moments in the un-magnetized iron structure*

The size of the domains fluctuates significantly between the values of 0.1 mm^3 to 1 mm^3.The magnetic domains are arranged so as to reduce entire the applied field. Like this, it keeps the energy level as low as could be allowed. Nearby domains follow this principle and have completely different magnetic moments, as appeared in Figure 3.2. Furthermore, the closure domains decrease the net external field.

In each crystal, boundaries split the domains from one another. These boundaries are termed as Bloch walls or domain walls. Figure 3.3 shows that, the magnetic moments change their direction in the opposite way across the domain walls. The depicted process of adding the magnetic moments of the atoms produces the impulsive magnetization of domains in the ferromagnetic materials, which is legitimate until a particular temperature. This particular temperature is called the Curie temperature T_c. The atomic thermal oscillations of a magnetic material increase with rise of temperature of the material. When the temperature increases above a certain level, then the thermal oscillations defeat the coupling forces that uphold the arrangement of the atomic magnets in the domains. The adjacent atoms face the interruption in the alignment of their magnetic moments. The magnetic properties of the ferromagnetic material become similar to a paramagnetic material as the temperature of ferromagnetic material rises above its Curie temperature.

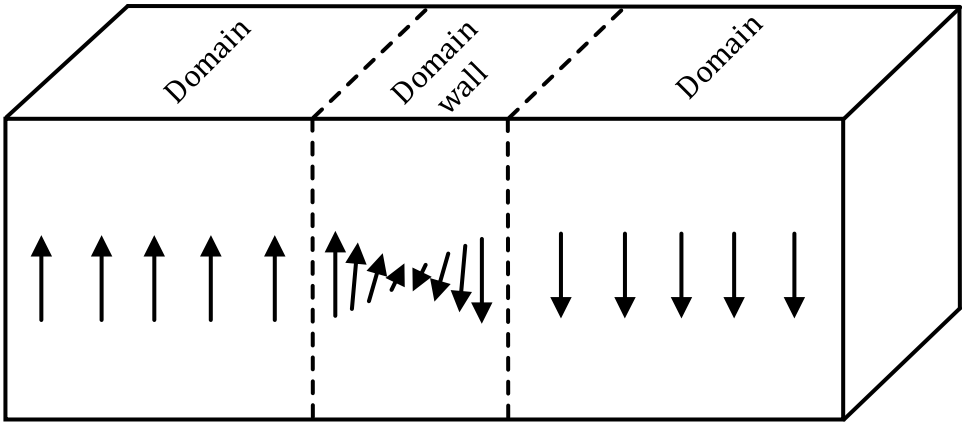

Figure 3.3: *Alignment of magnetic moments of material within an 180^o domain wall*

The remanence and coercivity drop to zero when the permeability of the material becomes $\mu_r = 1$. At the point when the material is cooled down, the alignment of the atomic magnets will restore but their position will be irregular to each other. The ferromagnetic material will be demagnetized if the temperature of the material increases more than T_c and hence the total applied field becomes zero in the structure [3].

3.1.2 Magnetization

The numerous domains are present in a crystal of a ferromagnetic material. The direction and magnitude of the imposed external field defines the magnetic arrangement, size and shape of the domains.

Figure 3.4a, shows a ferromagnetic material piece, which is unmagnetized. When an external magnetic field H_{ext} applies parallel to the magnetic domain moments, the domain walls start to shift. The movement of the domain walls increases with the strength of the applied field. The atomic magnets are exposed to torque as soon as an exterior field is applid. The applied field defines the alignment of the magnetic moments and arranges them in its direction. The aligned magnetic moments do not face any resulting torque. The non-aligned magnetic moments face torque and it forces them to rotate in the direction of the external applied field. Thus, the complete structure of domain wall gets the tendency to move. The net magnetic flux will produce in the crystal piece of ferromagnetic material, when the domains having the same direction as the applied external field H_{ext} expand into adjacent domains, which are aligned opposite to the field as shown in Figure 3.4b. Hence, the magnetization of all the atomic moments will increase and it is average value per unit volume.

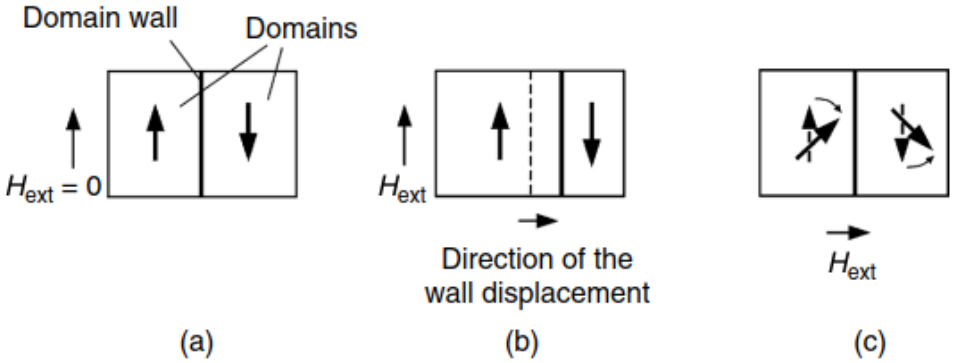

Figure 3.4: *Magnetization of a ferromagnetic sample: (a) no applied external field; (b) with applied (c) rotation of the domain magnetic moments under applied external field* H_{ext} [3].

The defined domain wall displacements turn out to be reversible at the point where the external applied field has a lower value. The greater value of the applied field H_{ext} causes hysteresis due to the displacements of walls. The rotation of the domain walls takes place as soon as the external applied field crosses over a specific level as shown in Figure 3.4c. A domain, which has the same direction of the external field, depletes a nearby domain who has the opposite direction to that field, it happens due to the domain wall jumps. At the point when the value of external field H_{ext} expands more, the procedure of rotation of the domain takes place. The schematic of 180 and 90 domain walls are shown in Figure 3.5. The 180^o wall movement causes alterations in the magnetization at low applied field and 90^o wall movement is responsible for alternations at the high applied field [18].

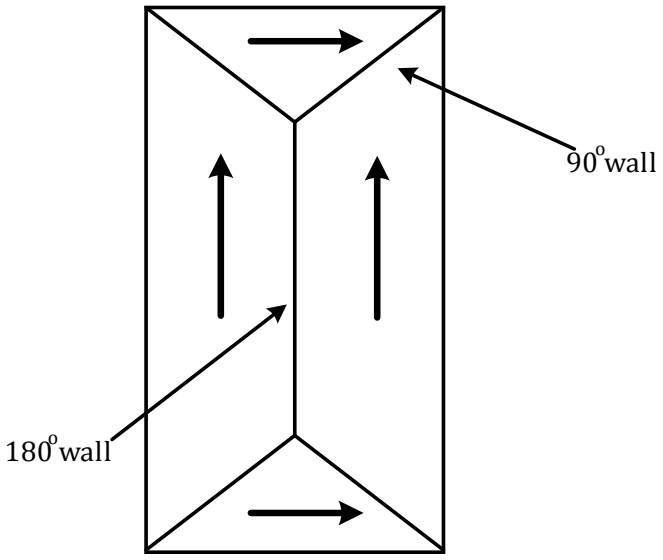

Figure 3.5: *Illustration of* 180^o *and* 90^o *domain walls*

The magnetization grows as soon as the magnetic domain moments spin to arrange themselves in the direction of the external field. Regardless of the original direction besides the crystal axes, the process has a tendency to arrange the magnetic domains further along the applied field. Domain spins, domain wall movements and jumps take place in the whole magnetization mechanism. Concerning ferromagnetic metals, the magnetization process starts with wall movements and jumps and it finishes with the spins of the entire domains, achieving the final arrangement in the approved direction, determined by the applied field [3].

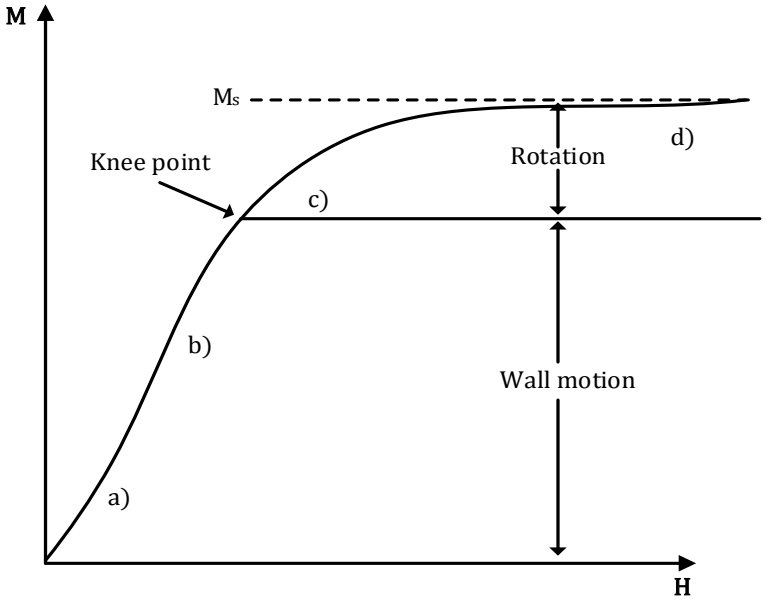

Figure 3.6: *The different phases of magnetization process due to the rotation of magnetizing vector and domain wall movement* [19].

The initial magnetization curve and the different phases of the magnetization process are presented in Figure 3.6. Between the demagnetic state and knee point, the magnetization process is controlled by the domain wall displacement. The reversible process happens when the external field is low, which displaces the domain wall. The domain wall comes back to position (a), when there is no external field. As soon as the external field increases at the position (b), the domain wall displacement turns into irreversible. The magnetization process modifies to irreversible rotation at temperate field strength. The applied field is now capable of rotating the domain at the position (c). Further increase in the applied field creates the reversible rotation of magnetic moments causing changes in the magnetization along the direction of the applied field (d). Real materials have different curves for growing and reducing fields and the motion of the domain walls is irreversible [16][19]. A simplified illustration of the magnetizing processes is shown in Figure 3.7.

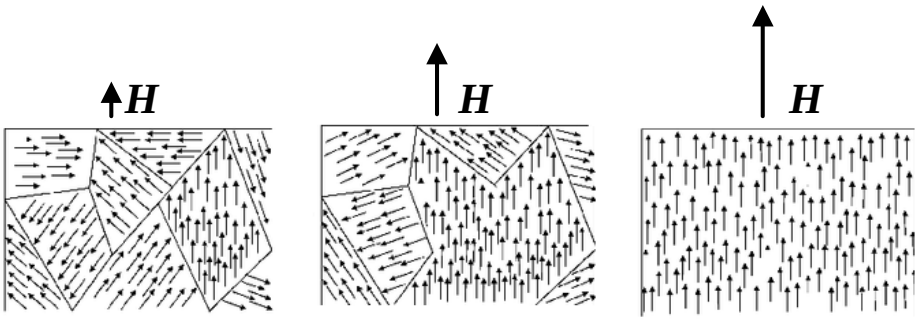

Figure 3.7: *Effect of the external magnetic field on domain walls*[19].

3.1.3 Magnetostriction

The ferromagnetic material faces a fractional change in its length when an external magnetic field is applied. This effect is termed as magnetostriction. The magnetostriction $\lambda_{\mathrm{m}}$is defined as

$$\lambda_{\mathrm{m}} = \frac{dL}{L} \tag{3.1}$$

where dL represents the change in length and L characterizes the initial length of the material sample. A spontaneous change in length dL arises when the temperature of the material is lower than the Curie temperature. The spontaneous magnetostriction and field-induced magnetostriction are the two types of magnetostriction. When the magnetic moments gather into the domains at the Curie temperature, it gives rise to produce spontaneous magnetostriction. If the affected domains rearrange further under the applied magnetic field, then it will produce field-induced magnetostriction resulting in a change in fractional length as shown in the Figure 3.8 [16].

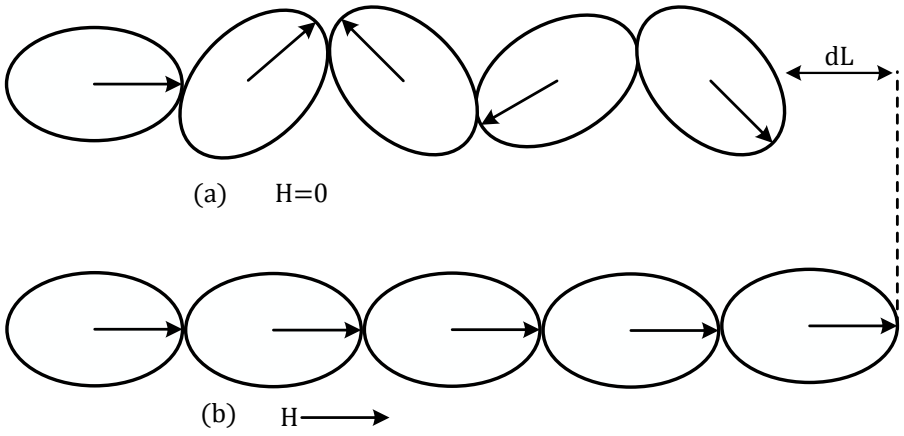

Figure 3.8: *Illustration of the magnetostriction under applied magnetic field* [16].

The value of λ_m at magnetic saturation is known as the saturation magnetostriction λ_s. Magnetostriction happens in almost every pure material. However, the strong magnetic materials have less magnetostriction effect. The saturation longitudinal magnetostriction λ_s can be negative or positive and some alloys have a zero value of λ_s at a certain temperature. The applied field and magnitude of magnetization determine the value of λ_s. The materials who have positive values of λ_m usually their dimensions increase under the applied magnetic field. Whereas the materials with negative magnetostriction usually contract. Due to the movement of the 90^o walls in the regions where the field is weak, the magnetostrictive fractional change in length produce.

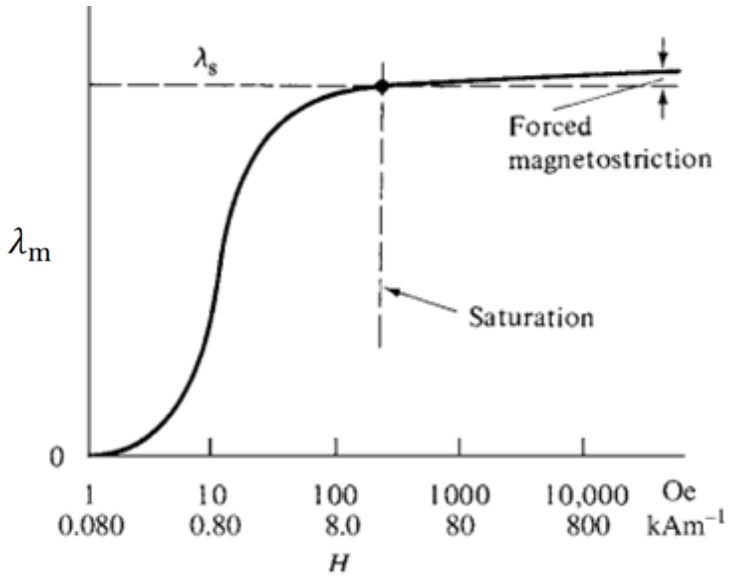

Figure 3.9: *Dependence of magnetostriction on magnetic field. Note that the field scale is logarithmic* [19] .

The variation of λ_m with H for a material of positive magnetostriction is shown in Figure 3.9. The maximum change in magnetostrictive length arises all along domain rotation. The volume of the sample remains approximately constant between the demagnetized point and saturation point. At the point when the technical saturation point approaches a certain temperature, the magnetic material sample changes into a single domain magnetized in the direction of the applied field. When the applied field rises more, it produces a slight additional strain. It yields a gradual variation in λ with H termed as forced magnetostriction. Under the applied field, when a slight variation happens in the volume after the saturation point, the resulting magnetostriction is termed as volume magnetostriction. This volume magnetostriction produces an equal shrinkage or expansion in all directions. Forced magnetostriction is a little impact and does not matter to the act of magnetic materials in standard fields [19].

3.1.4 Remanence

When a magnetic material is magnetized and then the applied magnetic field becomes zero afterwards. The magnetic flux remaining in the material is called the remanent flux B_{r} and remaining magnetization is known as the remanent magnetization M_{r}.

$$B_{\mathrm{r}} = \mu_o M_{\mathrm{r}} \tag{3.2}$$

The remanence is utilized to specify the value of any of the remaining magnetization or the magnetic flux when the field becomes zero after the magnetic material has reached the saturation point.

3.2 Soft and hard magnets

The types of ferromagnetic material depend on their coercive force H_{c} and those are soft magnetic material and hard magnetic material [3]. The alteration in the arrangement of the material structure defines the soft magnetic material and results in a narrow hysteresis B-H loop and low coercive force. A classic B-H loop of a soft magnetic material and a hard magnetic material is presented in Figure 3.10. The soft magnetic materials have lower values of coercive force compared with hard magnetic materials.

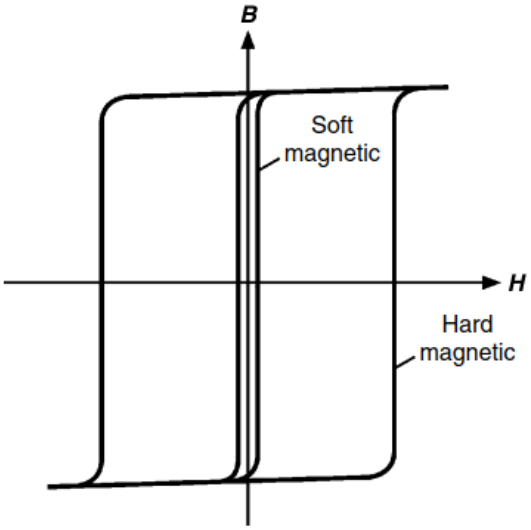

Figure 3.10: *Hysteresis loops: a narrow loop represents soft magnet and square loop denotes hard magnets*[3].

Hard magnetic materials are also known as permanent magnets. More of the external magnetic field is required to initiate the alignment of the magnetic moments of hard magnetic materials. The values of coercive force in permanent magnets are $H_{\mathrm{c}} > 10\ 000\ \mathrm{A/m}$ and in soft magnetic materials are $H_{\mathrm{c}} < 1000\ \mathrm{A/m}$. Hard magnetic materials are difficult to magnetize compared with soft magnetic materials and they have higher values of the

remanence induction B_r [3]. The examples of soft magnetic materials are represented in Figure 3.11.

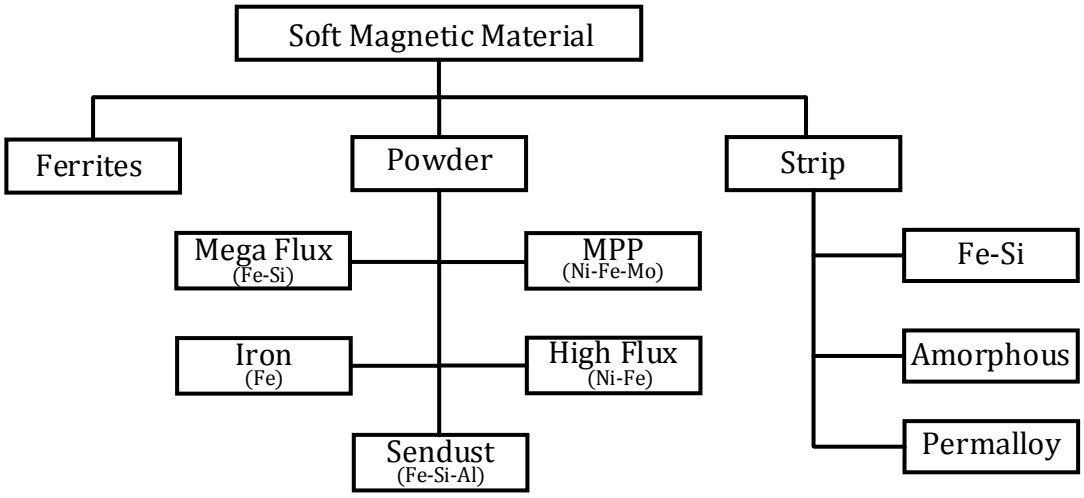

Figure 3.11: *Examples of soft magnetic materials*

4. INVESTIGATED MATERIALS

The focus of this thesis is merely on soft magnetic materials such as amorphous, nanocrystalline, molypermalloy powder (MPP), and ferrites.

4.1 Amorphous alloy

Amorphous alloys or soft magnetic materials are also called metallic glass. They are made of the metals cobalt, boron, manganese, silicon, nickel, niobium and alloys of iron. The structure of amorphous alloys depends on their chemical, mechanical, and magnetic properties.

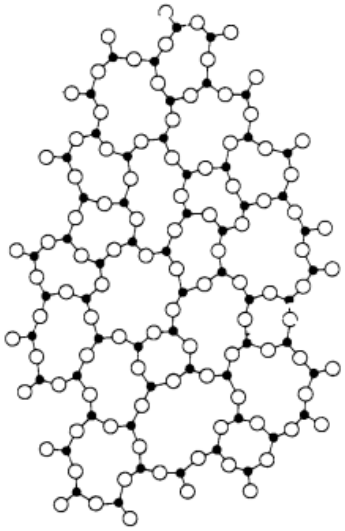

Figure 4.1: *Atomic structure of an amorphous material* [20]**.**

The amorphous has no crystalline structure and atoms in its structure are not in the order. The illustration of an amorphous atomic structure is shown in Figure 4.1. The alloys are formed with thin strips straight from a melt. The 1300°C hot molten is then compressed and cooled to a certain level [3]. Typically, amorphous has a composition of (Fe + Co + Ni) 80%, (Si + B) 20 %. In order to maintain the structure of amorphous, Si and B metalloids are for glass composition [19]. Amorphous materials have low coercivity and a linear trend of hysteresis loops. The maximum saturation induction of amorphous is 0.7-1.8 T. The range of Curie temperatures for the amorphous materials is 350–450°C. The magnetic properties start to disappear at this temperature.

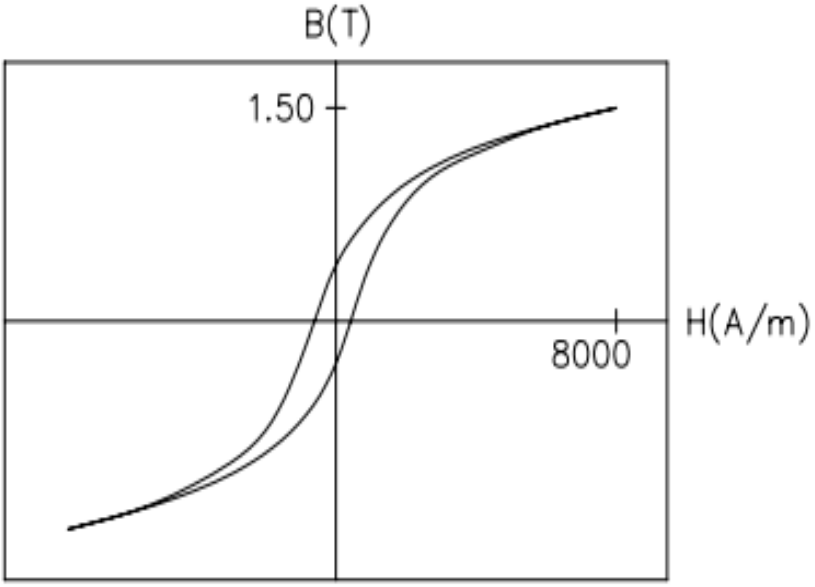

Figure 4.2: *Typical B-H loop of Metglas 2605SA1 toroidal core* [21].

For this thesis, Metglas amorphous alloy 2605SA1 is used. Amorphous alloy 2605SA1 is produced with thin ribbons typically around 23 µm thick and from about 142 mm to 213 mm wide. According to the material safety data sheet of Metglas 2605SA1, the composition of the alloy is as follows: iron 85 -95%, silicon 5-10% and boron 1-5% and it has a saturation flux density of 1.56 T [22][23][21]. The typical B-H loop of magnetic material 2605SA1 is shown in Figure 4.2.

4.2 Nanocrystalline material

Much work has been completed in the recent decade to represent new soft magnetic materials. These materials are named nanocrystalline materials. Yoshizawa from Hitachi Metals Laboratory created the first nanocrystalline material in 1988 [24]. The composition of nanocrysatalline initially suggested is $Fe_{74}\,Cu_{1}\,Nb_{3}\,Si_{15}\,B_{7}$. The Cu is supposed to increase nucleation of crystallites and the Nb to prevent their development [19]. The atomic structure of a crystalline sample is shown in Figure 4.3. An annealing process under the existence of a longitudinal or transversal magnetic field creates the nanocrystalline structure.

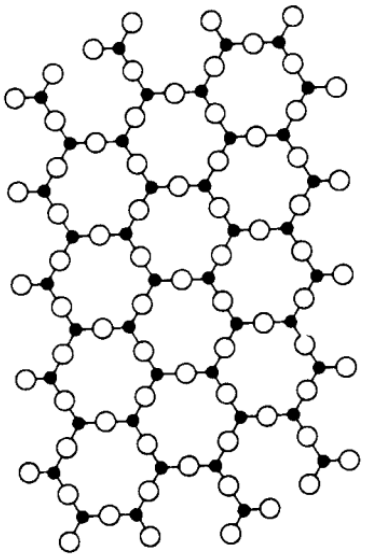

Figure 4.3: *Illustration of a crystalline atomic structure* [20].

The magnetic properties are influenced by the thermal treatment. As a result, the amorphous state faces a structural change [3]. Figure 4.4 represents the process of formation of amorphous ribbon for FINEMET® and a typical FINEMET® core. The pioneer material of FINEMET® is the amorphous ribbon. A “single roll method” is used to make this ribbon of thickness of 18µm and then a toroidal core is made by wounding these amorphous ribbons. Then the core undergoes a thermal treatment for crystallization.

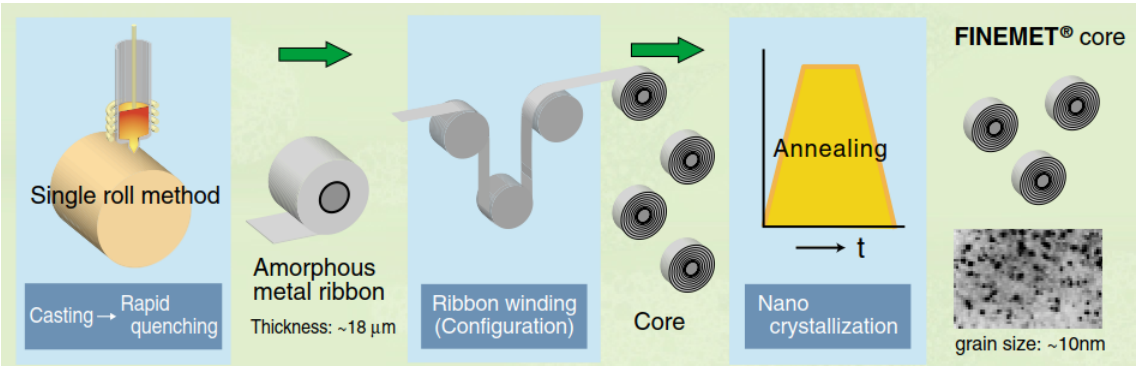

Figure 4.4: *Manufacturing process of FINEMET®* [25].

In the last stage of the crystallization process, the stabilized remaining amorphous phase at the grain boundaries suppresses the grain progression. The increase in the crystallization temperature of the remaining amorphous phase is the cause of this stabilization and stabilization increases with the enhancement of Nb and B [25]. The crystallization process of FINEMET® is shown in Figure 4.5.

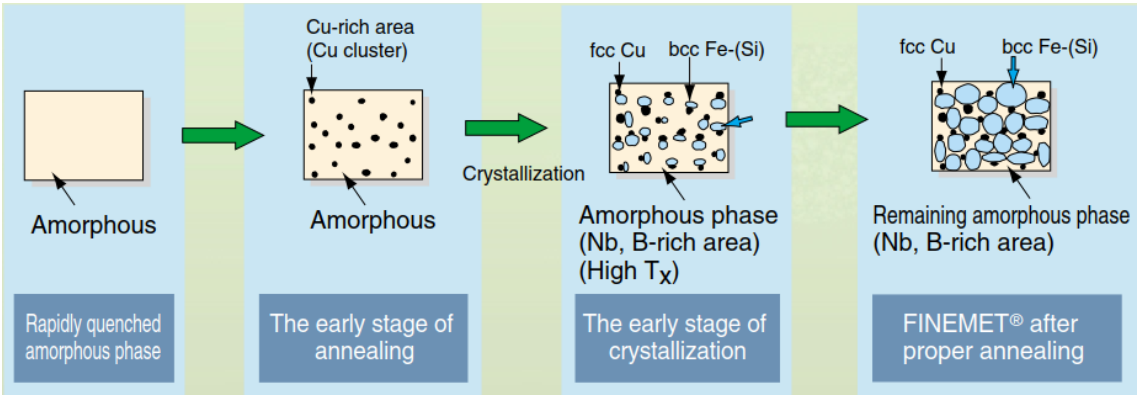

Figure 4.5: *Crystallization process of FINEMET®* [25]**.**

The typical B-H loop for the toroidal core of nanocrystalline FINEMET® FT-3M material is shown in Figure 4.6.

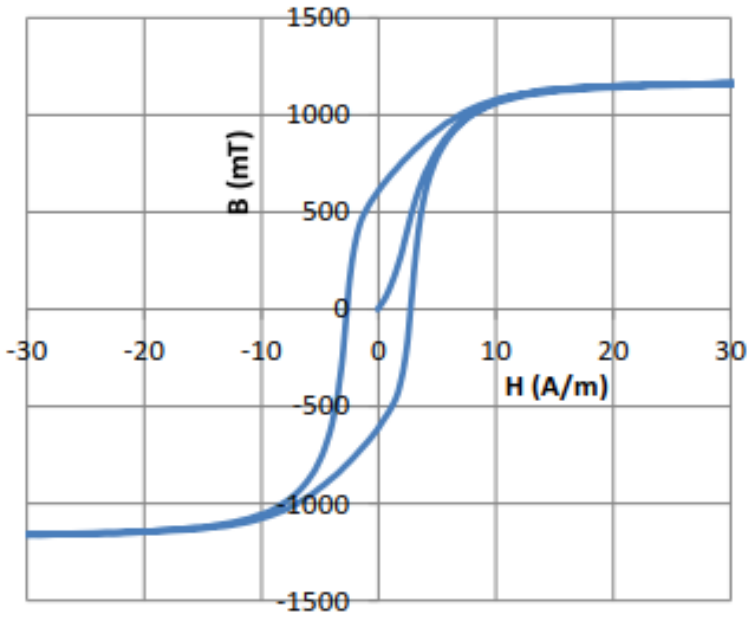

Figure 4.6: The *B-H loop of FINEMET® FT-3M toroidal material* [26].

4.3 Molypermalloy powder (MPP)

The powder material can consist of various chemical components to get the required properties of the core. The air gap is uniformly spread in the powder core rather than a gapped part in a standard ferrite core [27]. A lower flux leakage and better temperature steadiness come with the distributed air gap in the material. They additionally have a smoother decrease of their permeability, but it begins considerably earlier than in ferrites. From an EMI perspective, they are equally fine since a distinct air gap can affect other sections of the system. The particle size of powder material is related to the permeability of the core

and the greater the particle size, the higher the permeability will be. The molypermalloy powder (MPP) material has a composition of 17% iron, 81% nickel and 2% molybdenum alloy powder. Among the other powder cores, MPP has minimum losses and it is utilized when lowest losses are required. Under dc magnetization, MPP cores maintain their inductance stability, high resistivity, low hysteresis losses and low eddy current losses [28]. The dc magnetizing curves of MPP material at different permeabilities are shown in Figure 4.7.

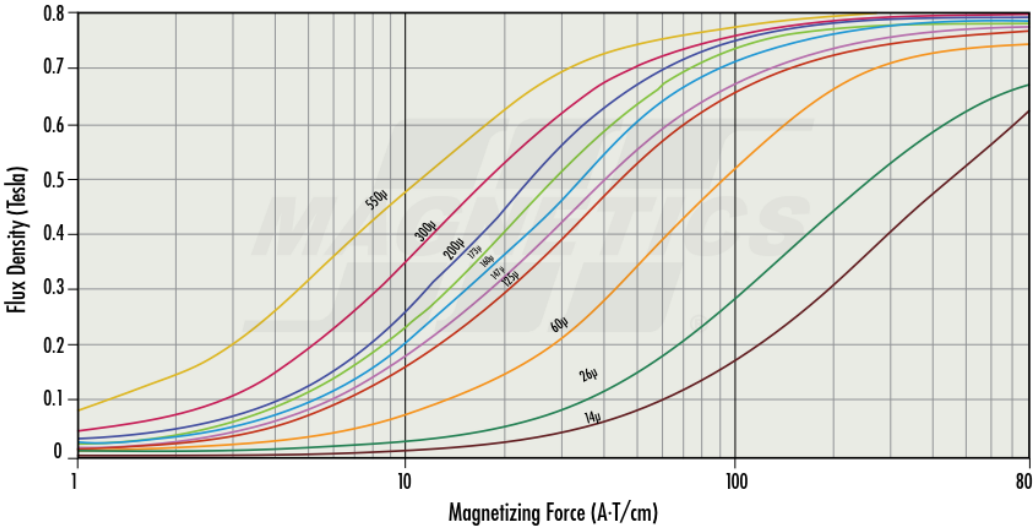

Figure 4.7: *The dc magnetizing curves of MPP material at different permeabilities* [28].

4.4 Ferrites

Ferrites are the most commonly utilized materials in the field of power electronics. The high volume resistivity of the ferrites is their main characteristic and distinguishes them from the other magnetic materials. Eddy current losses are directly proportional to the square of the frequency and inversely proportional to the resistivity. Because of the high resistivity, ferrites can be used commonly in high frequency magnetic applications [3]. The typical B-H loop of ferrite F-material is shown in Figure 4.8.

The ferrite materials are made of iron oxide Fe_2O_3 and have a cubic crystal structure. Typically, they combine with other metals like silicon, magnesium, nickel, copper, zinc and cobalt. The Mn-Zn and Ni-Zn are the two common categories [19]. Due to the high permeability of Mn-Zn materials, their operating range of frequency is up to 5 MHz. On the other hand, Ni-Zn have a high resistivity and lower permeability and they can be used in higher frequency applications [29].

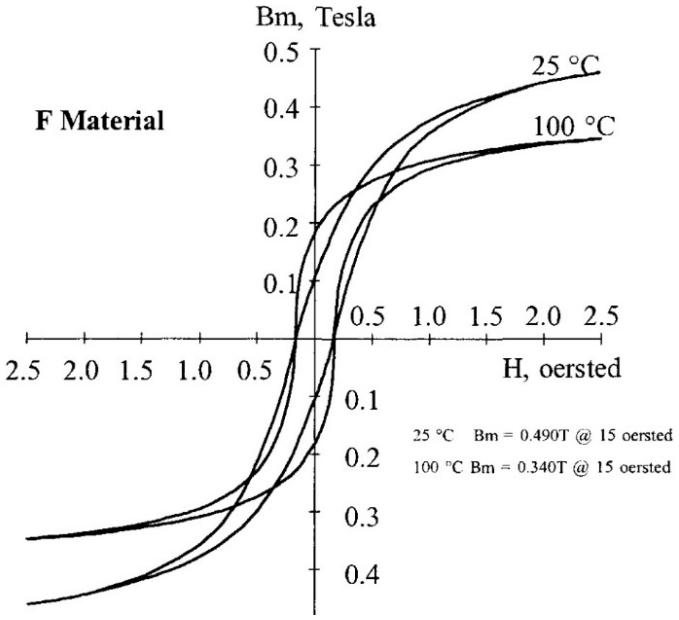

Figure 4.8: *The B-H loop of F Material at 25° and 100° C* [7].

The MAGNETICS® F material is useful for the power filters, transformers and inductor's material and can be used for medium frequency applications [30].

5. DESIGNING OF TEST INDUCTOR CORES

In many circumstances, the inductor can be used for storing magnetic field energy. It's ability of storing magnetic field energy can be exploited in different areas of the field. For example, the magnetic field is utilized in electric machines to transfer energy through air from a static region to a non-static region. In another case of electric fences, where an inductor is utilized to collect energy with time before losing it to produce an instantaneous voltage spike. The purpose of this section is to design an inductor in order to achieve the required magnetic flux density and magnetic field intensity.

5.1 Shapes of cores

The core shapes influence the performance of an inductor. Inductors are intended for many applications with various prerequisites. The E-core, pot core, C-core and a toroidal core are the basic examples of core shapes are shown in Figure 5.1 [31].

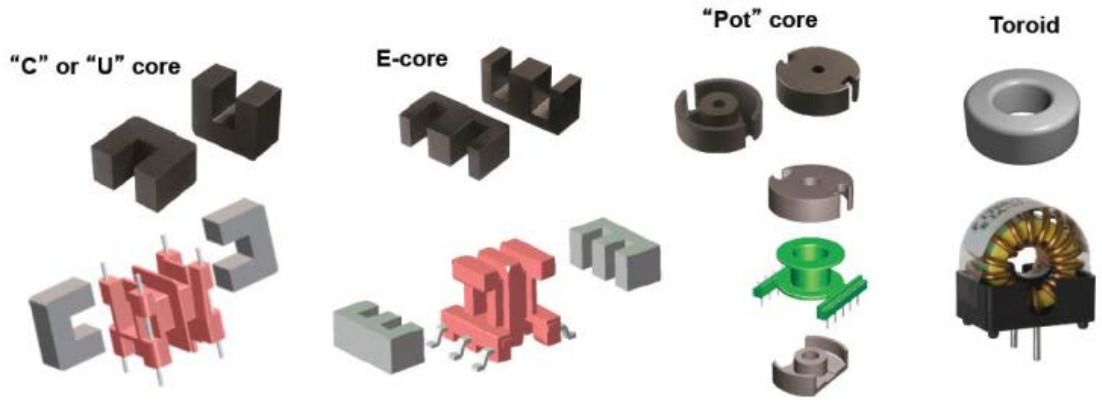

Figure 5.1: *Basic shapes of different cores* [31].

Each shape has its different benefits and disadvantages and to pick a suitable shape depends upon the application. The focus of this thesis is on toroidal cores. The maximum magnetic field is enclosed inside the toroidal core. The basic shape of a toroidal core is shown in Figure 5.2, where *OD* represents the outer diameter, *ID* is the inner diameter, A_e is the effective area of the core cross section, l_c is the mean magnetic path length and *h* is the height of the toroidal core.

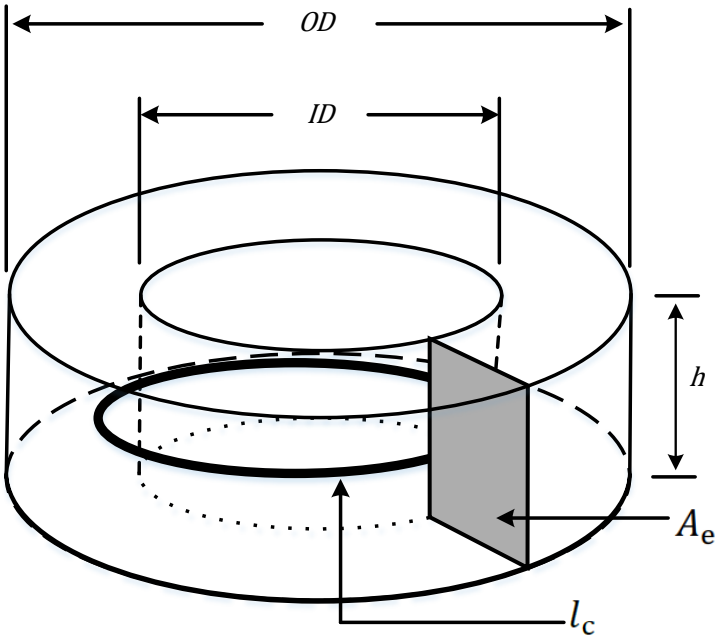

Figure 5.2: *Typical structure of a toroidal core* [32].

5.2 Toroidal inductor design considerations

Among the devices of power electronics, inductors are considered the utmost vital components. Their usages in the EMC chokes, magnetic energy storage, current limiters and filters make them significant. Magnetic inductor designing is a complicated issue, where magnetic and electrical aspects must be considered before designing. The winding loss, current densities, wire insulation, temperature of the core, currents, current densities, frequency, voltages, proximity and skin effect are the main features from the electrical perspective. Permeability of the core, saturation flux density, saturation current, inductance, dimension and cross sectional area of the core are the key features from the magnetic prospective [33]. The leakage flux is very small in toroidal cores due to their symmetry. On the other hand, if magnetic flux is not limited inside the core then it can cause the eddy currents, electromagnetic interference and the flux leakage in the adjacent conductors [34]. The aim of this study is just to measure the material properties at high flux density, not to design an inductor at a given value of inductance. For this purpose, the design consideration steps are as follows:

1. Selection of the investigated materials
2. The values of peak flux density B_{pk} and field intensity H are selected from the dc magnetizing curves of the materials.
3. Selection of cores and geometry properties
4. Defining the number of primary and secondary turns
5. Calculation of flux path length

6. Voltage and current calculations
7. Winding calculations
8. Power loss calculations

Properties of material and current are the main aspects, which affect the size of the inductor. The magnetic saturation of the core should be considered during the design because it can create problems of inductance loss, current rise and extra power loss in the circuit [33]. The flux path length is calculated with the following equation.

$$l_{\mathrm{c}} = \frac{(OD + ID)\pi}{2} \tag{5.1}$$

The magnetic flux path is used to calculate the primary currents with (2.27) and then voltages are computed by using (2.25). The specification of the power amplifier used in the proposed measurement setup is limited. It provides a maximum current of 30 A at 156 V and 15 A current at a voltage of 312 V. If the current and voltage calculations do not fall in these criteria then the step#3 and step#4 are reconsidered. Usually, when the length of wire is shorter than one meter with a few number of turns, then the maximum rms current density under room conditions is between 6 A/mm^2 to 10 A/mm^2. For a length of the wire longer than one meter and larger number of turns, the maximum rms current density can be 5 A/mm^2 [6]. The area of cross sectional of primary wire A_{wp} is calculated with selected wire diameter by

$$A_{\mathrm{wp}} = \pi \left(\frac{d_1}{2}\right)^2 \tag{5.2}$$

where d_1 is the bare wire diameter. The current density J_{rms} is calculated by

$$J_{\mathrm{rms}} = \frac{I_{\mathrm{p\_rms}}}{A_{\mathrm{wp}}} \tag{5.3}$$

The core geometry defines the length of the wire and number of turns per layer. The length of one turn is

$$l_{1\mathrm{turn}} = (OD - ID) + 2h \tag{5.4}$$

where h is the height of the core. The total primary wire length $l_{\mathrm{p\_w}}$ is calculated as

$$l_{\mathrm{p\_w}} = l_{1\mathrm{turn}}\, N_1 \tag{5.5}$$

where N_1 is the total number turns of primary winding. The resistivity ρ of the wire material, total length of the wire l_{wp} and wire cross sectional area define the dc resistance of the primary wire $R_{\mathrm{p\_dc}}$. The dc resistance $R_{\mathrm{p\_dc}}$ of the wire is given as

$$R_{\mathrm{p\_dc}} = \rho \frac{l_{\mathrm{p\_w}}}{A_{\mathrm{wp}}} \tag{5.6}$$

Then the resultant total copper loss $P_{\mathrm{Cu\_p}}$ of primary wire is calculated as

$$P_{\mathrm{Cu\_p}} = I_{\mathrm{p\_rms}}^2 R_{\mathrm{p\_dc}} \tag{5.7}$$

5.3 Core design examples

The typical characteristics of the investigated materials are given in Table 5.1. The amorphous 2605SA1 has the highest saturation magnetic flux density among other core materials.

Table 5.1: *Summary of materials properties* [21]–[23], [25], [26], [28]–[30], [35].

Material type	Material	Manufacturers	Permeability	Saturation flux density (T)	Curie temperature (°C)
Amorphous	2605SA1	Metglas	245	1.56	395
Powder	MPP	Magnetics	200	0.8	460
Ferrite	F	Magnetics	3000	0.47	210
Nanocrystalline	FT-3M	Hitachi Metals	10000	1.23	570

However, the nanocrystalline FT-3M material has the highest permeability and Curie temperature. Moreover, it has excellent characteristics but it is costly related to other materials. The MPP material and ferrite F material have lower saturation flux densities and lower Curie temperature.

Table 5.2: *The properties of the toroidal cores* [21], [26], [36], [37].

Symbol	Parameter	Amorphous	MPP	Ferrite	Nanocrystalline
OD	Outer diameter (mm)	46.61	58.04	61.85	79.7
ID	Inner diameter (mm)	25.22	34.74	36.53	50.3
h	Height (mm)	18.99	14.9	12.96	25.7
A_{c}	Cross-section area (mm^2)	143	144	157.4	150
l_{c}	Magnetic path length (mm)	112.8	145.7	154.5	204.2
V_{c}	Volume (mm^3)	15800	20700	22774	771500
B_{pk}	Peak flux density (T)	1.45	0.7	0.4	1

Table 5.3: *The specifications of wire used for toroidal cores.*

Symbol	Parameter	Amorphous	MPP	Ferrite	Nanocrystalline
N_1	No. of primary turns	80	200	50	10
N_2	No. of secondary turns	20	50	50	20
d_{p}	Nominal primary wire diameter (mm)	0.6	1.18	0.6	0.5
d_{s}	Nominal secondary wire diameter	0.3	0.18	0.3	0.3
A_{wp}	Area of bare primary wire (mm^2)	0.2827	1.094	0.283	0.196
A_{ws}	Area of bare secondary wire (mm^2)	0.707	0.0706	0.0706	7.069

5.3.1 Amorphous core

The specifications of the MP7438MDGC core and its geometry are given in Table 5.2. The following calculations are done using 50 Hz frequency. The wire properties are given in Table 5.3. The peak flux density $B_{\mathrm{pk}} = 1.45$ T is considered from the B-H curve of amorphous 2605SA1 material as shown in Figure 4.2. In addition, the corresponding value of the magnetic field strength is $H = 7000$ A/m . The calculated rms current in the primary winding is $I_{\mathrm{p\_rms}} = 6.98$ A. The length of one winding turn is given as $l_{1\mathrm{turn}} = 0.0594$ m and total length of the primary wire is $l_{\mathrm{p\_w}} = 4.749$ m. The dc resistance of the primary wire is $R_{\mathrm{p\_dc}} = 0.28\ \Omega$. The primary voltage is $V_{\mathrm{p\_rms}} = 5.64$ V. Some voltage is dropped because of the dc resistance of the wire and this is also included in the calculated primary voltages. The total primary winding loss is calculated as $P_{\mathrm{cu\_p}} = 13.64$ W. The total length of the secondary winding is $l_{\mathrm{s\_w}} = 1.187$ m and the secondary voltage is $V_{\mathrm{s\_rms}} = 0.92$ V. The test design of amorphous 2605SA1 core is shown in Figure 5.3.

Figure 5.3: *The prototype of 2605SA1 amorphous core.*

5.3.2 MPP core

The IEC 60317-0-1 standard of copper wire is used in designing the inductor. The peak flux density $B_{\mathrm{pk}} = 0.7$ T is assumed from the B-H curve of MPP material as shown in Figure 4.7. In addition, the corresponding value of magnetic field strength is taken $H = 6000$ A/m. The specification of MPP C055106A2 core and winding are given in Table 5.2 and Table 5.3 respectively. The rms current in the primary winding is $I_{\mathrm{p\_rms}} = 3.09$ A. The length of one winding turn is given as $l_{1\mathrm{turn}} = 0.0531$ m and total length of the primary wire is $l_{\mathrm{p\_w}} = 10.62$ m. The dc resistance of the primary wire is $R_{\mathrm{p\_dc}} = 0.1679\ \Omega$. The primary voltage is $V_{\mathrm{p\_rms}} = 4.97$ V. The total primary winding loss is calculated as $P_{\mathrm{cu\_p}} = 1.547$ W. The total length of the secondary winding is $l_{\mathrm{s\_w}} = 2.655$ m and the secondary voltage is $V_{\mathrm{s\_rms}} = 1.12$ V. The test sample of the MPP core is shown in Figure 5.4.

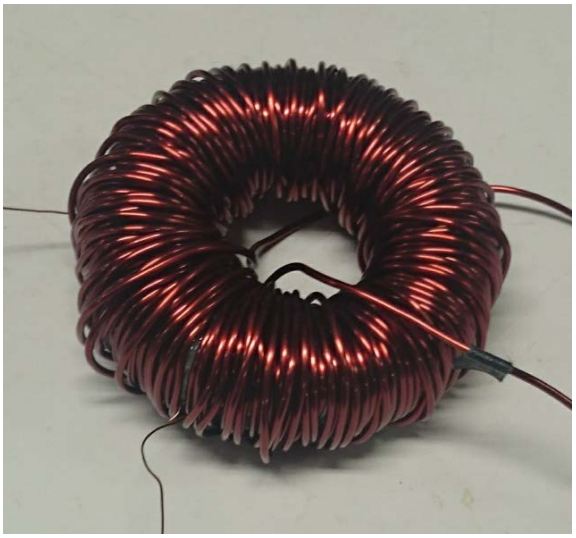

Figure 5.4: *The prototype of MPP core.*

5.3.3 Ferrite core

The designing of the inductor also depends on the dimension of the core geometry. The saturation flux density of the ferrite material is $B_{\mathrm{sat}} = 0.47$ T. The peak flux density $B_{\mathrm{pk}} = 0.4$ T is taken from the magnetizing curve of the ferrite material given in Figure 4.8 and the magnetic field strength is considered from the same curve is $H = 119.4$ A/m. The specification of the core geometry is represented in Table 5.2 and the specifications of the windings are characterized in Table 5.3.

The rms current in the primary winding is calculated as $I_{\mathrm{p\_rms}} = 0.261$ A. The dimensions of ferrite are larger than the MPP C055106A2 core and amorphous MP7438MDGC core. The length of one turn is $l_{1\mathrm{turn}} = 0.0594$ m and the total length of the primary winding is $l_{\mathrm{p\_w}} = 2.562$ m. The resulting dc resistance of the primary winding is $R_{\mathrm{dc\_p}} = 0.1510\ \Omega$. The calculated primary voltage is $V_{\mathrm{p\_rms}} = 0.756$ V. The corresponding power loss in the primary winding is $P_{\mathrm{cu\_p}} = 0.0103$ W. The total length of the secondary winding is $l_{\mathrm{s\_w}} = 2.562$ m and the secondary voltage is $V_{\mathrm{s\_rms}} = 0.7168$ V. The prototype of the ferrite core is shown in Figure 5.5.

Figure 5.5: *The prototype of ferrite material core.*

5.3.4 Nanocrystalline core

The saturation flux density is $B_{\mathrm{sat}} = 1.23$ T for the nanocrystalline material and it has the highest permeability among the other cores. The peak flux density $B_{\mathrm{pk}} = 1$ T has been chosen from the B-H loop of the nanocrystalline FT-3M material shown in Figure 4.6 and the magnetic field strength is considered from the same curve is $H = 8\ \mathrm{A/m}$. The specification of the FT-3KMF7555G core is given in Table 5.2.

The specification of designed windings for the nanocrystalline core is given in Table 5.3. The nanocrystalline core has the highest core geometry and it takes the lowest current to magnetize. The rms current in the primary winding is calculated as $I_{\mathrm{p\_rms}} = 0.116$ A. The length of one turn is $l_{1\mathrm{turn}} = 0.081$ m and total length of the primary winding is $l_{\mathrm{p\_w}} = 0.808$ m. The resulting dc resistance of the primary winding is $R_{\mathrm{dc\_p}} = 0.068\ \Omega$.

The calculated primary voltage is $V_{\mathrm{p\_rms}} = 0.341$ V. The resulting power loss in the primary winding is $P_{\mathrm{cu\_p}} = 0.0009$ W. The total length of the secondary winding is $l_{\mathrm{s\_w}} = 1.62$ m and the secondary voltage is $V_{\mathrm{s\_rms}} = 0.67$ V. The test sample of nanocrystalline core is shown in Figure 5.6.

Figure 5.6: *The prototype of nanocrystalline core.*

6. MEASURMENT SETUP AND WORKING PRINCIPLE OF CALCULATING CORE LOSS

The measurements of magnetic materials are necessary for the characterization of their properties. The measurement equipment allows acquiring the curves of different kind like B-H loops, core losses curves and magnetization curves of different magnetic materials. This chapter presents a detailed overview of laboratory equipment used in the measurement setup and working principle. Moreover, it also contains the measurements of B-H loops for four different magnetic materials. The core losses were measured over 1 Hz to 1 kHz range.

6.1 Measurement setup

The block diagram of the experimental setup for measuring B-H curves and core losses is shown in Figure 6.1. A MATLAB code is developed to create VISA-USB interface between a pc and a KEYSIGHT DSO-X-3014T digital oscilloscope. This oscilloscope can be controlled and programmed by the MATLAB program.

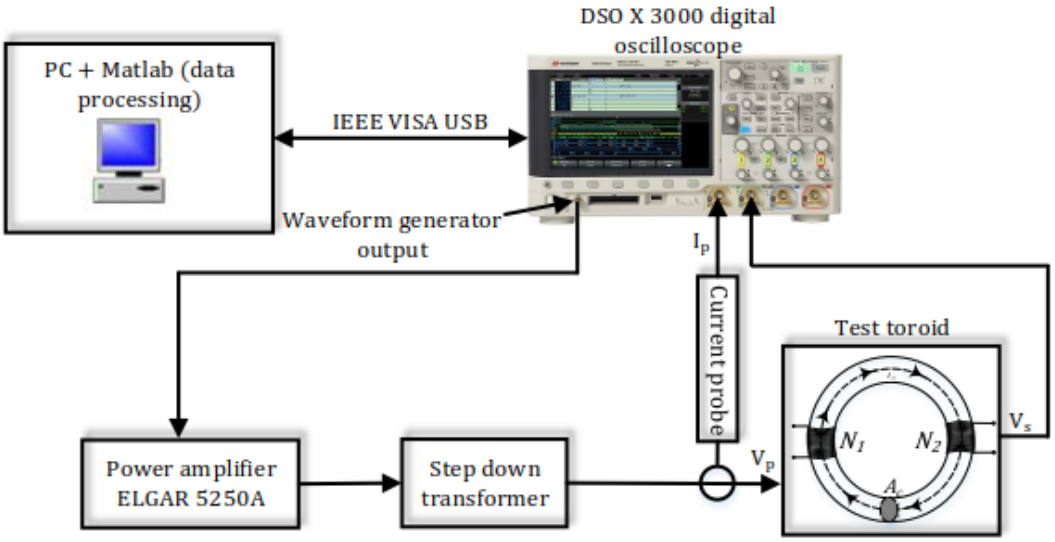

Figure 6.1: *Measurement setup for core loss.*

The output of the waveform function generator of the oscilloscope is a low power signal, it cannot magnetize the primary winding of the test toroidal core. A power amplifier (ELGAR 5250A) is used to amplify the signal and then the amplified signal is fed to the step down transformer to reduce the voltages required for the excitation coil. The excitation current is measured with a current probe, which is further connected to channel one of the oscilloscope and induced output voltage is measured at channel 2 of the oscilloscope. The

pc collects the measured data from the oscilloscope. Figure 6.2 represents the laboratory setup.

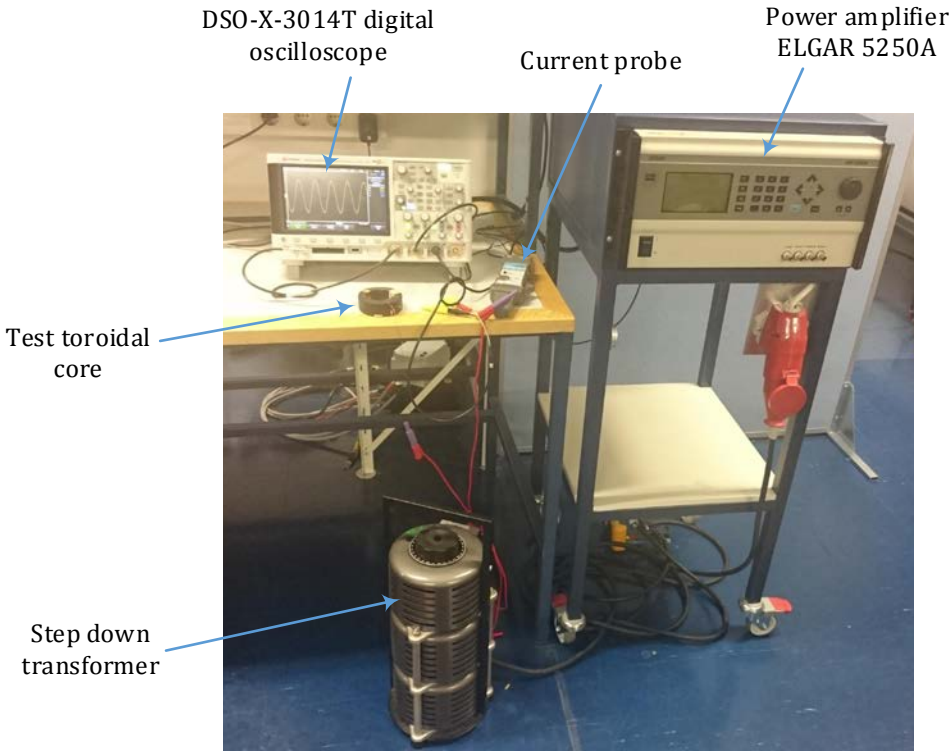

Figure 6.2: *Laboratory setup.*

6.2 Measurement principle for B-H loop and core loss

The magnetic material properties can be measured using a toroidal core [40]. Different methods which can be used to measure core losses and B-H loop, are developed in [4], [40], [5], [41], [42]. The core loss method developed in [4] and [5], is utilized in this study. According to [4], if the area of cross section of the core is not uniform, *B* and *H* will not remain uniform in the material. This will result in difficulty reading the data. The core has two windings, a primary winding (excitation winding) and a secondary winding (sensing winding). The primary winding is utilized to produce the magnetic field intensity *H*.

The purpose of the secondary winding is to measure the voltage for deriving magnetic flux density *B*. A single winding could be enough for the measurements, but the current will cause a voltage drop over its internal resistance and it further leads to measurement error. The primary winding is fed an rms ac supply voltage from the transformer while the sensing winding is an open circuit and no current flows in it. The current is measured at the primary winding using a current probe and the voltage is measured at the secondary

side with an oscilloscope as shown in Figure 6.1. The magnetic flux density is obtained by integrating the voltage of the sensing winding:

$$B(t) = \frac{1}{N_2 A_c} \int v_s dt \tag{6.1}$$

The core loss per unit volume is given by

$$p_{loss} = \frac{N_1}{N_2 A_c l_c} \frac{1}{T} \int_0^T v_s i_p dt \qquad {}^{W}/_{m^3} \tag{6.2}$$

The sensing voltage $v_s(t)$ and excitation current $i_p(t)$ contain dc offsets due to the measurement errors and power supply. These offsets were removed by calculating the mean values of the sensing voltage and excitation current signal and subtracting them from their original signal. The dc offset is also removed from the calculated magnetic flux density $B(t)$. The readings were measured from zero to the maximum flux density and approximately 500 samples per cycle were recorded. The proposed method is used to obtain the B-H curves (Figure 6.3) and the core loss per unit volume for a test core material in Figure 6.4.

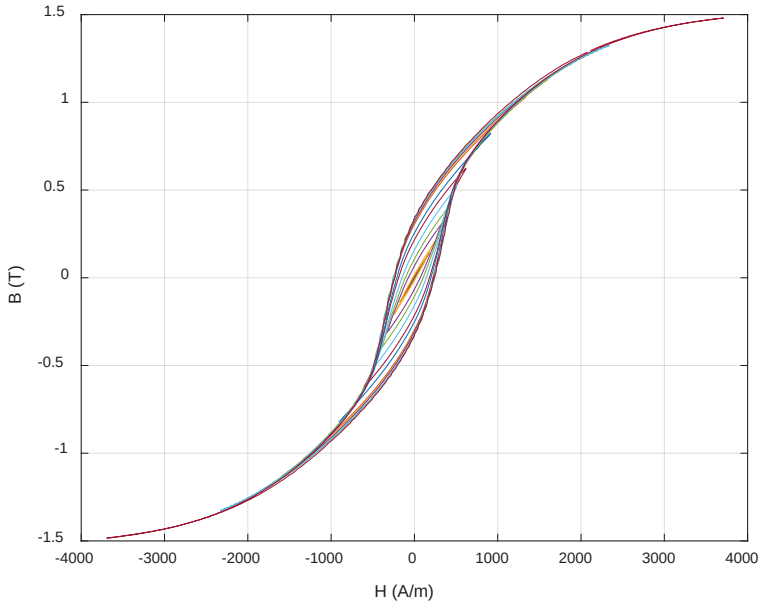

Figure 6.3: *The B-H loops of a test sample at 50 Hz.*

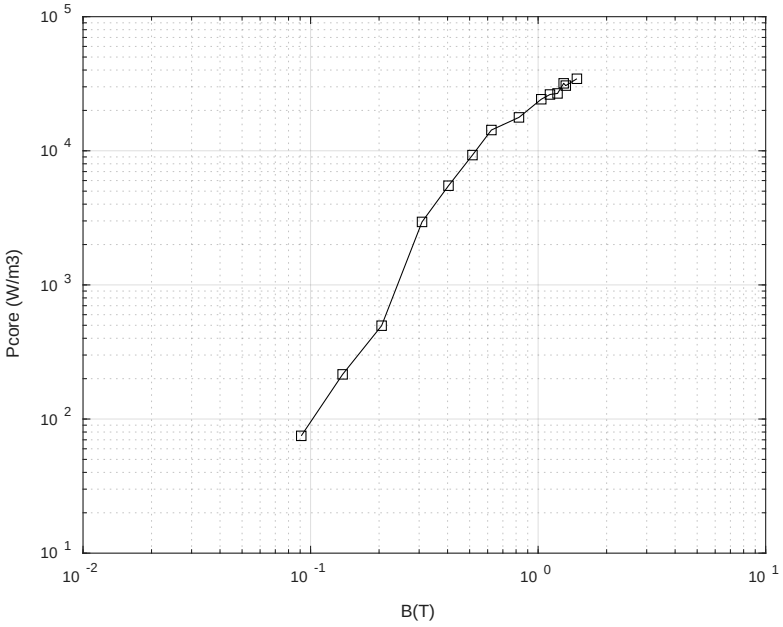

Figure 6.4: *Core loss per unit volume of a test sample at 50 Hz.*

The dc magnetizing curve is obtained by plotting the peak values of magnetic flux density against magnetic field intensity as shown in Figure 6.5.

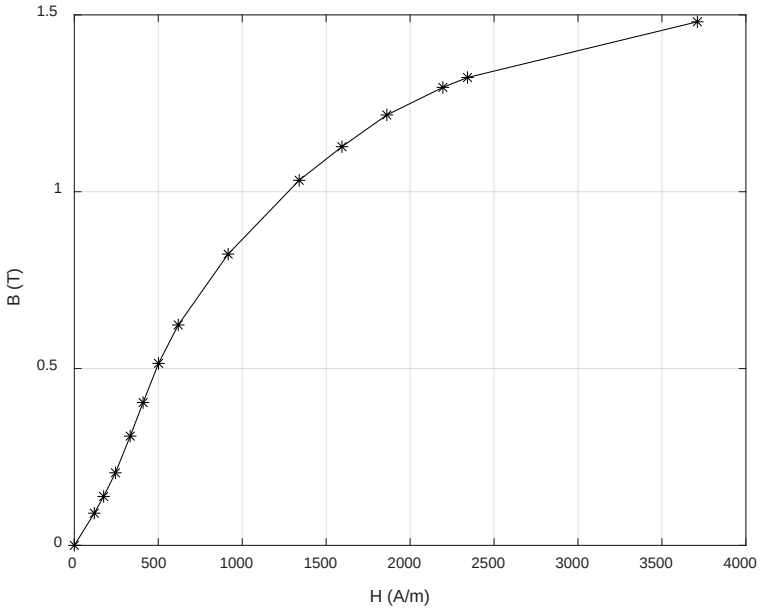

Figure 6.5: *Dc magnetizing curve of a test sample at 50 Hz.*

7. RESULTS AND DISCUSSION

This section explains the results obtained from the experimental measurements. The measurement method explained in Chapter 6 was applied to get B-H loops and hysteresis losses for the test materials. Four different toroidal cores were made for the measurement purpose. Their dimensions and characteristics are explained in Chapter 5. The measurements were taken for different magnetic materials. The core losses of ferrite, MPP, nanocrystalline and amorphous materials were measured up to 1 kHz frequency. The aim was to measure losses up to high magnetic flux density values. The magnetic flux density B values were achieved by increasing the excitation voltage in the primary winding.

7.1 Amorphous core

The core losses per unit volume in the amorphous core as a function of frequency at three different magnetic flux density values 0.4 T, 1 T, and 1.4 T are shown in Figure 7.1.

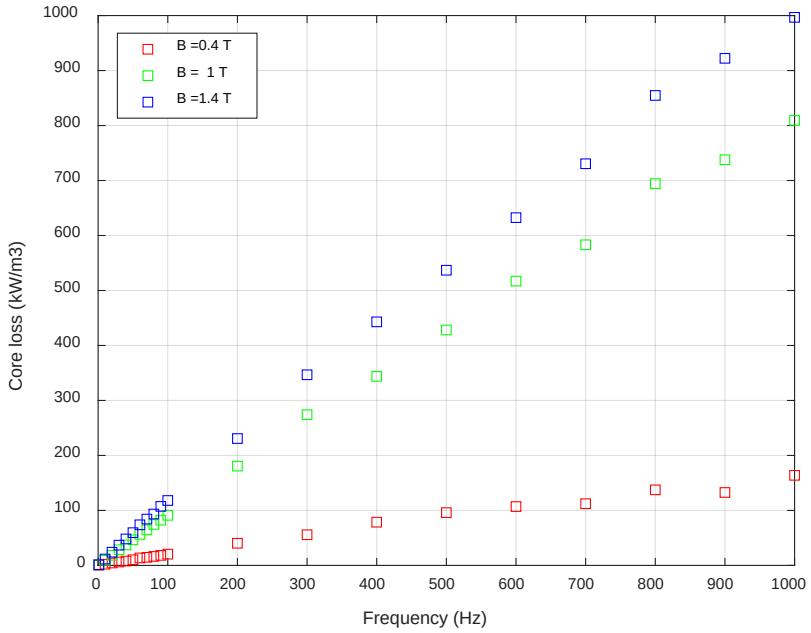

Figure 7.1: *Core loss per unit volume versus frequency for amorphous material.*

The measured data shows that the core loss density for the flux density B = 0.4 T rises slowly in comparison to other curves. For the curves of B = 1T and B =1.4 T, the core loss density trend is almost linear from 100 Hz onwards. The highest core loss for B = 1 T is $p_{\text{loss}} = 809.3\ \text{kW/m}^3$ and for B = 1.4 T is $p_{\text{loss}} = 996.7\ \text{kW/m}^3$. It can be noticed that, the core losses for B = 1.4 T are almost 10 times higher than for B = 0.4 T.

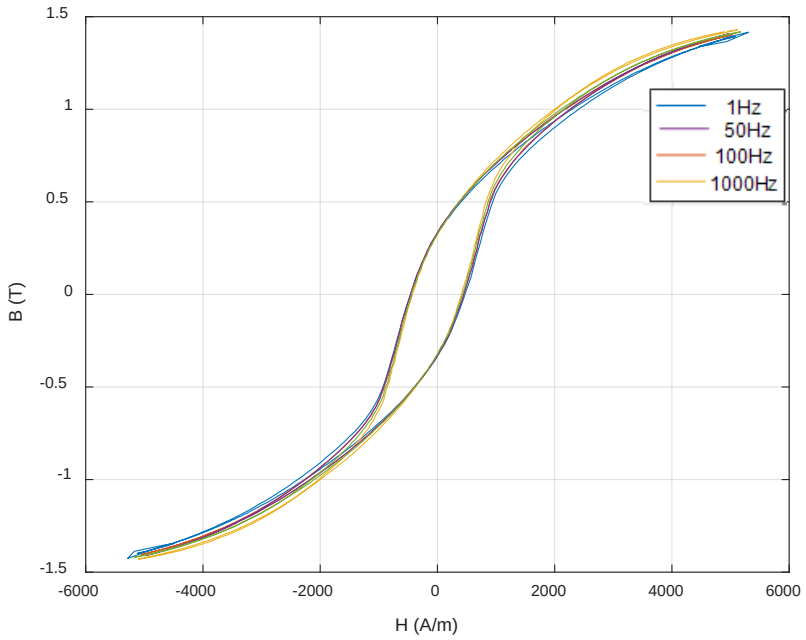

Figure 7.2: *The B-H loops at B = 1.4 T for amorphous core.*

The B-H loops for amorphous material at constant magnetic flux density are shown in Figure 7.2. The measured data shows that the frequency does not have too much effect on the area of the B-H loop. On the other hand, in Figure 7.3, it is clearly shown that at a constant frequency, the area of B-H loops increases with magnetic flux density.

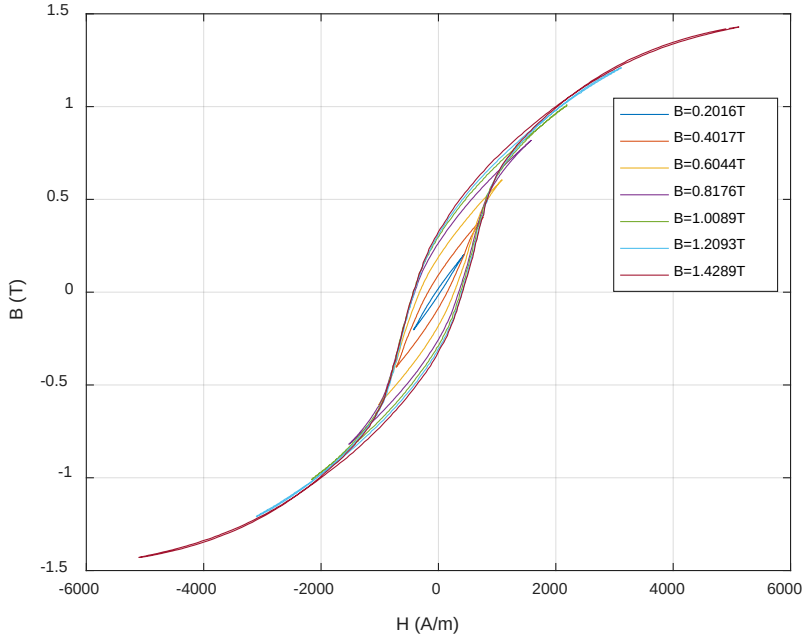

Figure 7.3: *The B-H loops at f = 1 kHz for amorphous core*

7.2 MPP core

The core losses per unit volume of an MPP core as a function of frequency are shown in Figure 7.4. For this core, the highest achieved flux density was 0.7 T. During the experiments with MPP core material, it was observed that the core was heating when it reached higher magnetic flux density. The decreasing trend in the core loss density is due to the temperature difference in the core. The core loss density at 1 kHz is lower than the core loss density at 900 Hz for the B = 0.7 T. This effect can also be seen in other core loss density curves.

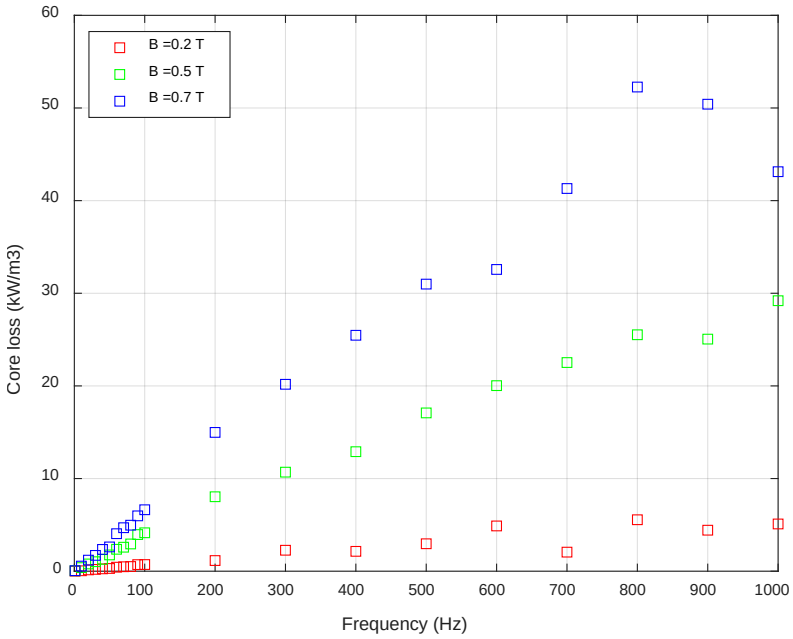

Figure 7.4: *Core loss per unit volume versus frequency for MPP core material.*

For the MPP core material, core losses increase with frequency and magnetic flux density values. The measurement data shows that the maximum core loss density is $p_{\text{loss}} = 52.3\ \text{kW/m}^3$ at $f = 800$ Hzand B = 0.7 T. However, the core loss density trend is non-linear due to the temperature effect in the core. The losses in the MPP core are 16 times lower compared to the losses in the amorphous core.

Figure 7.5 shows the heating effect in the core for three different frequencies at a constant magnetic flux density of B = 0.7 T. The measurements were taken in two ways.

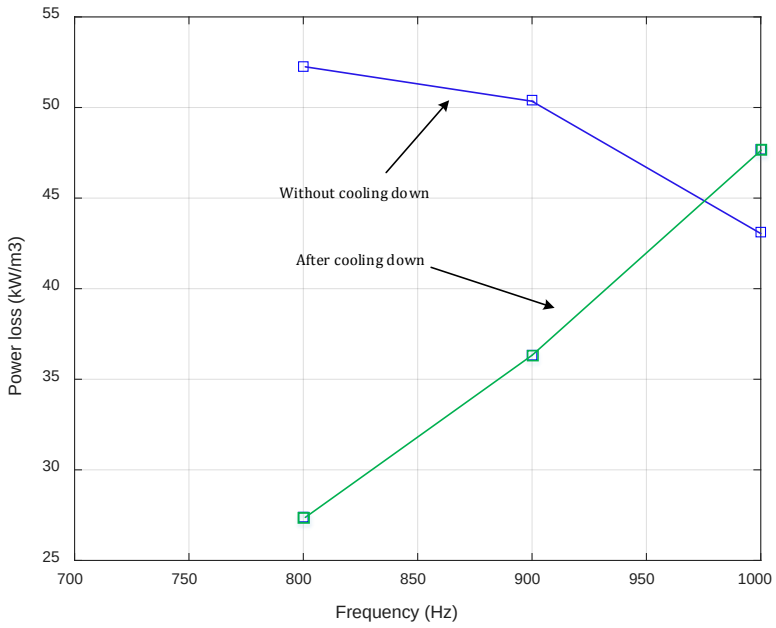

Figure 7.5: *Heating effect in MPP core at B =0.7 T.*

The blue curve represents that the measurements were taken without cooling down the core. For the green curve, the core was properly cooled down before starting any new measurement. It can be seen that the blue curve shows a decreasing trend because of the temperature difference in the core. The green curve of core loss density represents the increasing trend.

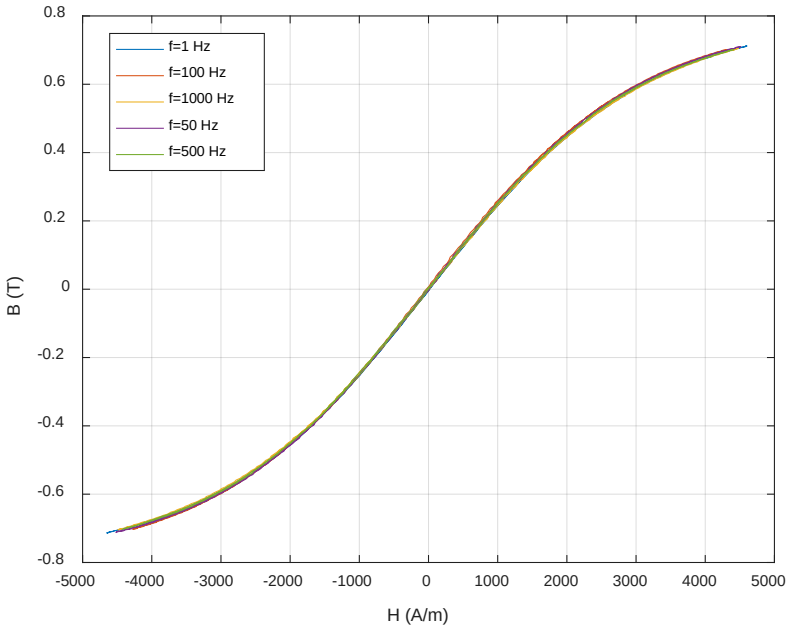

Figure 7.6: *The B-H loops at B = 0.7 T for MPP core.*

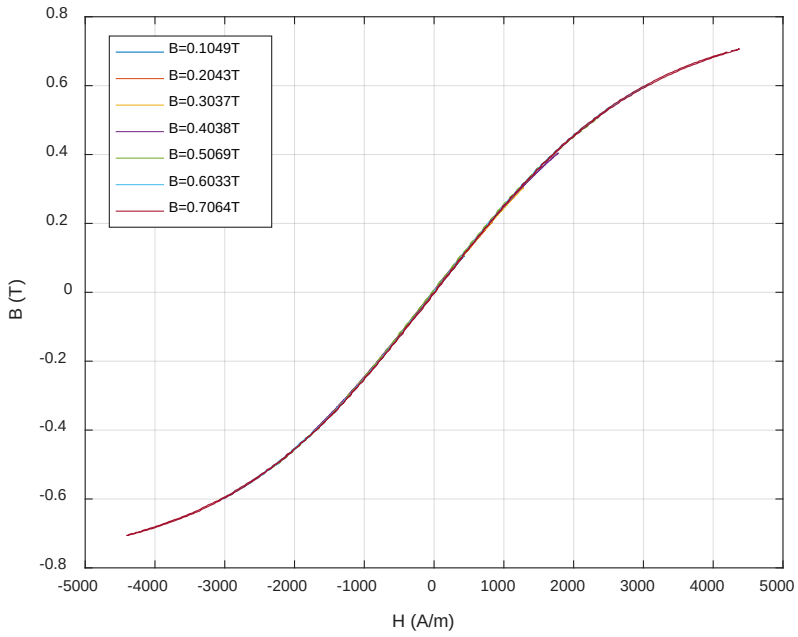

Figure 7.7: *The B-H loops at f = 1 kHz for MPP core.*

From Figure 7.6 and Figure 7.7, it can be clearly observed that the MPP core has very thin B-H loops, which is why the losses in MPP core are lower than the amorphous core.

7.3 Ferrite core

The core losses per unit volume of a ferrite core as a function of frequency at three different magnetic flux density values are shown in Figure 7.8.

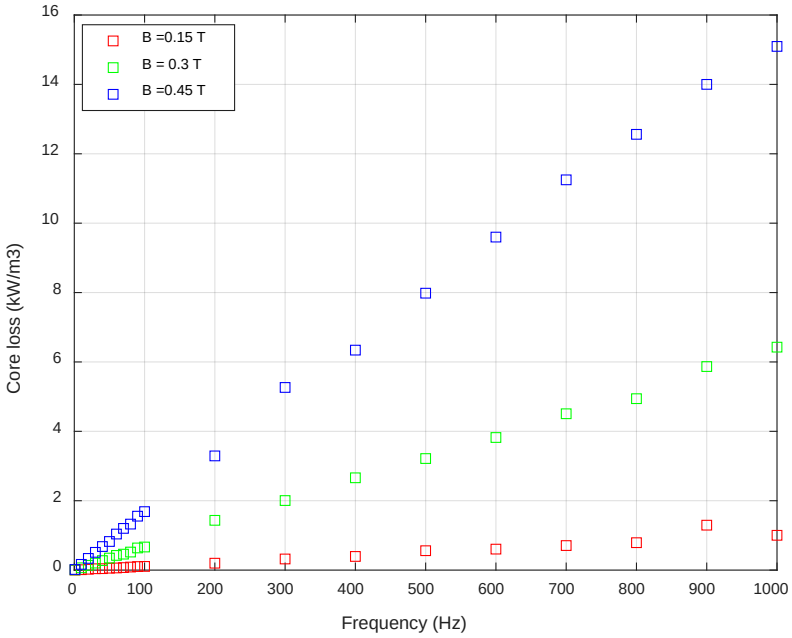

Figure 7.8: *Core loss per unit volume versus frequency for ferrite material.*

The measured data clearly shows that the ferrite core has the lowest loss compared with the other two cores, MPP core and amorphous core. The ferrite also has an almost linear trend of core loss density. The highest core loss density is measured at B = 0.45 T and $f = 1$ kHz, which is $p_{\text{loss}} = 15.1\ \text{kW/m}^3$.

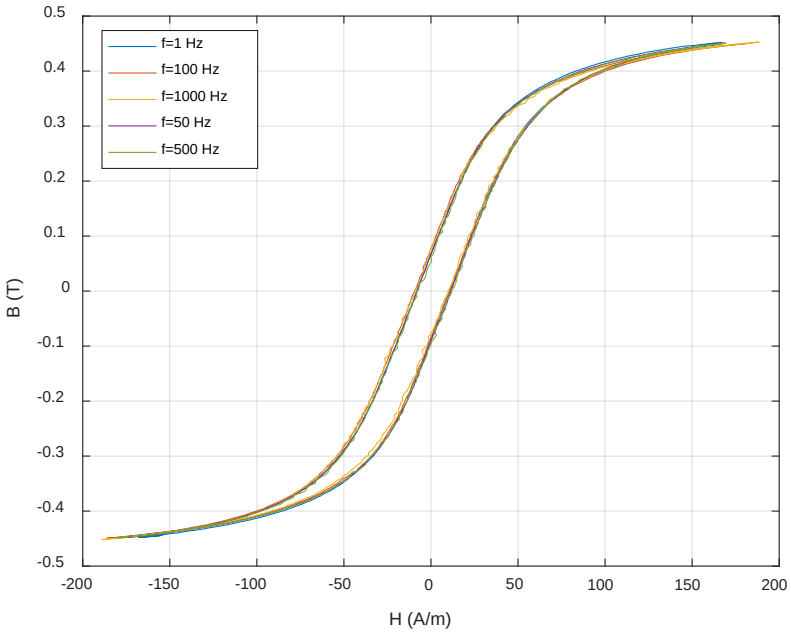

Figure 7.9: *The B-H loops at B = 0.45 T for ferrite core.*

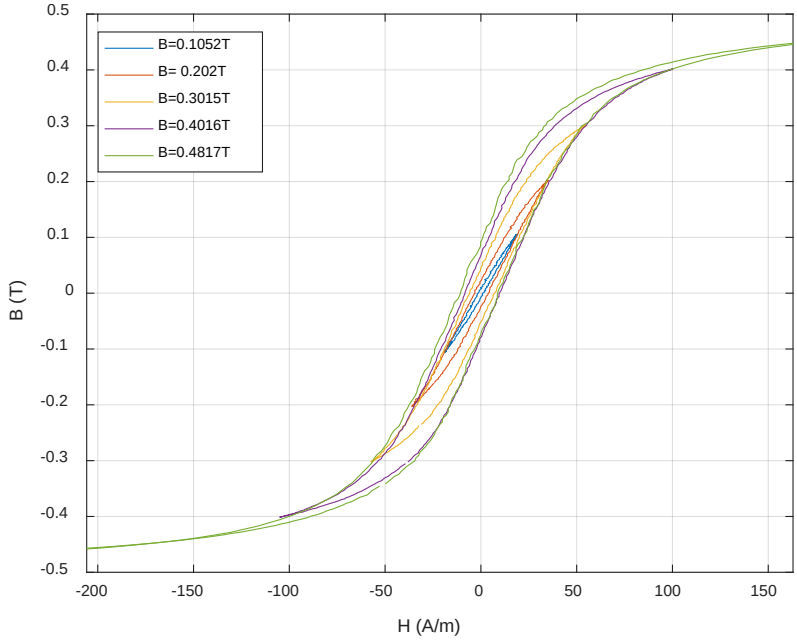

Figure 7.10: *The B-H loops at f = 100 Hz for ferrite core (zoomed).*

The B-H loops at constant magnetic flux density are shown in Figure 7.9. The measured data shows that frequency has not too much effect on the area of the B-H loop. The B-H loops at $f = 100$ Hz for the ferrite core are shown in Figure 7.10. It can be observed that the loop area increases with the rise of magnetic flux density and it produces more losses in the core.

During the measurements of the ferrite core, a remanence effect was observed in the core. Some magnetization remained in the core even after removing the excitation ac magnetic field, which caused the error in the measurement results. One of the reasons is that the output of the function generator cannot be zero. The output can be reduced to 20 mV maximum. Due to this, some remanence is still left in the core. To reduce the remanence effect in the core, first it was magnetized up to the highest value of magnetic flux density and then it was demagnetized by reducing the excitation voltage slowly. This process was repeated after each measurement of the ferrite core.

7.4 Nanocrystalline core

The measured core losses per unit volume against frequencies are shown in Figure 7.11. It can be noticed from the measured data that the nanocrsytalline core has the lowest losses among the other cores.

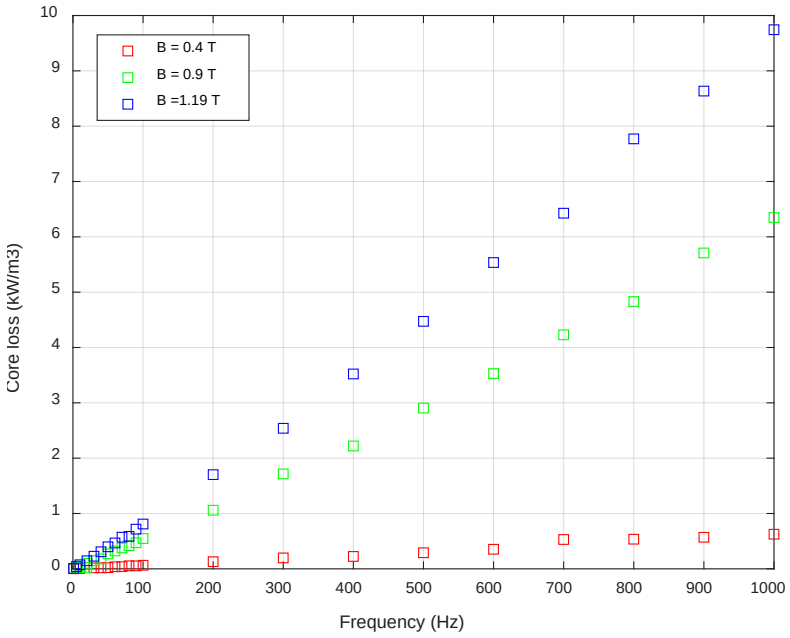

Figure 7.11: *Core loss per unit volume versus frequency for nanocrystalline material.*

The highest core loss density is measured at B = 1.19 T and f = 1 kHz, which is $p_{\text{loss}} = 9.74\ \text{kW/m}^3$. The core loss density curves for all three magnetic flux density values are

linear. It can be seen in Figure 7.12 that the loop area also increases with the frequency of excitation for the nanocrystalline core. The B-H loops at a constant frequency are shown in Figure 7.13. The measured data shows that the core has some remanence and loop area increases with rising magnetic flux density. Due to the limitations of the measurement setup, the maximum achieved value of magnetic flux density was 1.20 T.

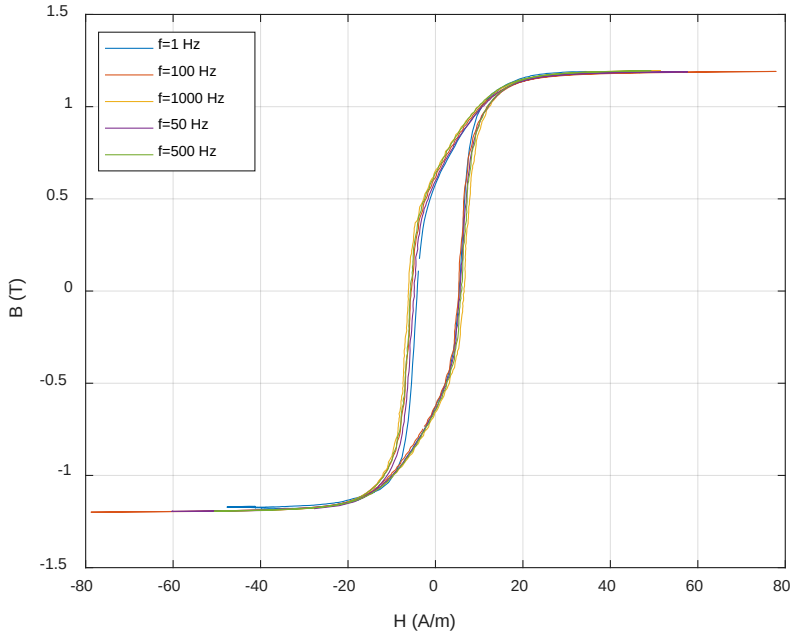

Figure 7.12: *The B-H loops at B = 1.19 T for nanocrystalline core.*

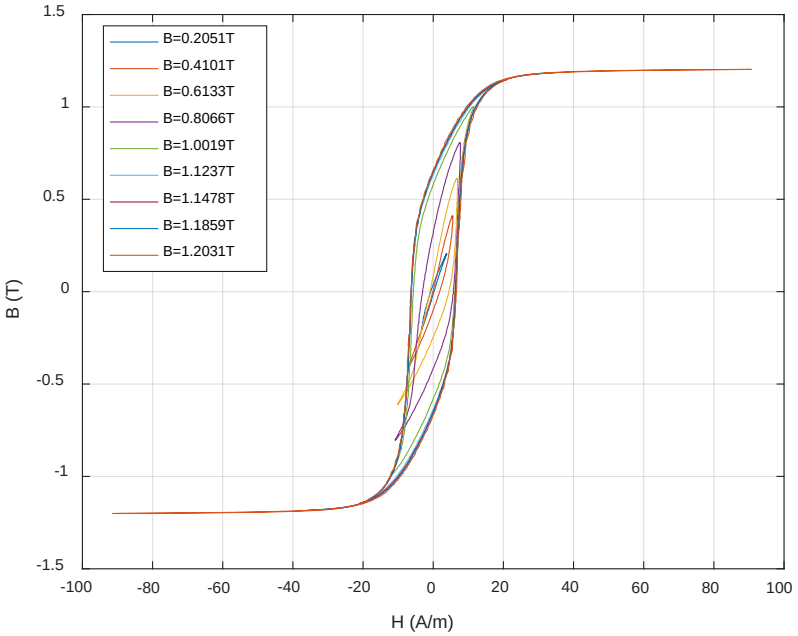

Figure 7.13: *The B-H loops at f = 1 kHz for nanocrystalline core.*

In the beginning, the measurements were taken by triggering the secondary winding voltage signal or primary current signal in the oscilloscope. The voltage and current signals were not triggered properly. Due to this problem, the data acquisition of the signals from the oscilloscope was not performed correctly, because the signals were not standing still. It further created the fluctuation in the core loss density curves. By triggering the clean signal (output of the waveform function generator) of the oscilloscope, the triggering problem was solved.

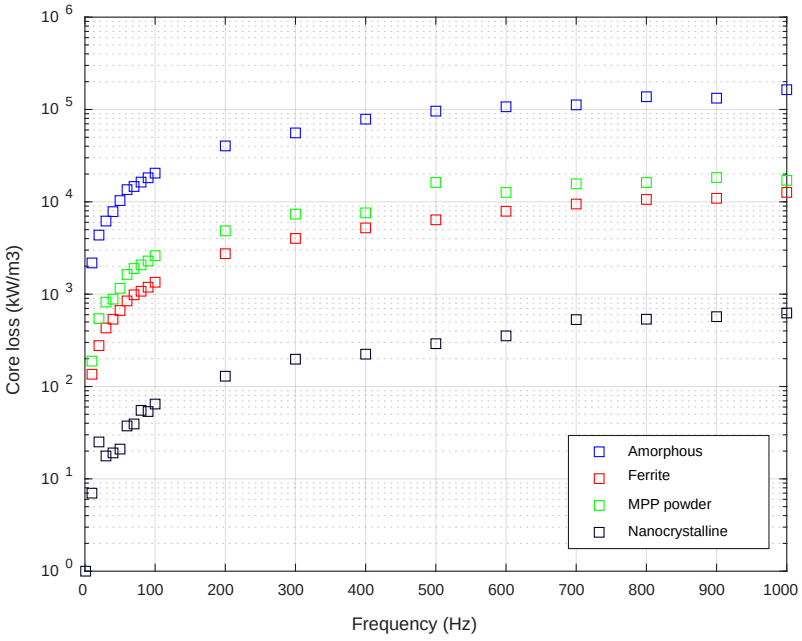

Figure 7.14: *Core loss density vs frequency for different materials at B = 0.4 T*

At a constant magnetic flux density value of 0.4 T, the core loss per unit volume for all core materials is shown in Figure 7.14. The experimental data shows the estimated increase of losses with frequency but with different curves. The amorphous has the highest slope. We can see that losses in ferrite are comparatively low, but they are almost double the losses in nanocrystalline core. The core loss density slope of MPP core is quite near to the slope of the ferrite core.

8. CONCLUSION

In this thesis, the core losses of four soft magnetic materials ferrite, molypermalloy powder (MPP), nanocrystalline and amorphous are measured under the sinusoidal voltage excitation up to a frequency of 1 kHz. The measurement method described in [4] and [5] are used to measure the core loss density and the B-H loops.

The measured data indicates that nanocrystalline has the lowest losses among other cores. It has the highest Curie temperature and can operate at high temperatures. It also has a high saturation flux density. It can be used in applications, where high magnetic flux density and high temperature is required. The ferrite core material shows lower losses than amorphous and MPP core material. The amorphous shows the highest core loss density among the other core materials. The measured data shows the dependency of core loss density on the flux density and frequency.

It was observed that remanence effect was dominant in the ferrite core when the applied magnetic field was zero. The nanocrystalline core also showed some remanence. From the experiments, it was concluded that in order to obtain better measurement results, any remaining residual flux in the core should be eliminated before starting any new measurement. First, a test core was magnetized up to the highest magnetic flux density and then it was demagnetized by reducing the excitation voltage slowly. This process was repeated after each measurement. In this way, residual flux was removed. In addition, the effects of temperature are not considered in the core loss measurements, which may have influenced the measured core loss results. Moreover, the magnetic flux density was not sinusoidal during the measurements, and thus it is not so straightforward to compare the values at different flux densities and frequencies.

The future work may focus on improving the measurement setup. The core losses of different soft magnetic materials can be analyzed with more appropriate measurement techniques. The cores should be measured in a cooling container in order to prevent them from heating.

REFERENCES

[1] A. J. Marin-Hurtado, S. Rave-Restrepo, and A. Escobar-Mejia, “Calculation of Core Losses in Magnetic Materials under Nonsinusoidal Excitation,” *Int. Power Electron. Congr. - CIEP*, vol. 2016–Augus, pp. 87–91, 2016.

[2] T. Kauder, K. Hameyer, “Performance Factor Comparison of Nanocrystalline, Amorphous and Crystalline Soft-magnetic Materials for Medium-frequency Applications,” *IEEE Trans. Magn.*, vol. PP, no. 99, pp. 1–1, 2017.

[3] A. V. D. Bossche, V. C. Valchev, “Inductors and Transformers for Power Electronics. ” Taylor & Francis groups, 2005.

[4] W. L. Soong, “B-H Curve and Iron Loss Measurement for Magnetic Materials,” *Power Eng. Brief. note Ser.*, vol. 5, no. May, pp. 5–6, 2008.

[5] J. Mühlethaler, J. Biela, J. W. Kolar, and A. Ecklebe, “Core losses under the DC Bias Condition Based on Steinmetz Parameters,” *IEEE Trans. Power Electron.*, vol. 27, no. 2, pp. 953–963, 2012.

[6] M. K. Kazimierczuk, “High-Frequency Magnetic Components,” 2nd edition, John Wiley & Sons Ltd, 2013.

[7] C. W. T. Mclyman, “Transformer and Inductor Design Handbook,” 3rd edition, Marcel Dekker, Inc., 2004.

[8] A. E. Fitzgerald, C. Kingsley, S. D. Usman “Electric Machinery,” 6th edition, McGraw-Hill Companies, Inc., 2003.

[9] W. H. Hurley, W. G. Wölfle, “Transformers and Inductors for Power Electronics Theory, Design and Applications,” John Wiley & Sons Ltd., 2013.

[10] Y. Gao, Y. Matsuo, and K. Muramatsu, “Investigation on Simple Numeric Modeling of Anomalous Eddy Current Loss in Steel Plate using Modified Conductivity,” *IEEE Trans. Magn.*, vol. 48, no. 2, pp. 635–638, 2012.

[11] P. C. Sen, “Principles of Electric Machines and Power Electronics,” 2nd edition, New York: John Wiley and Sons Ltd., 1997.

[12] N. Mohan, T. M. Undeland, and W. P. Robbins, “Power Electronics Converters, Applications, and Design,” 3rd edition, New York: John Wiley and Sons Ltd., 2007.

[13] R. W. Erickson and Dragan, “Fundamentals of Power Electronics,” 2nd edition, Kluwer Academic Publishers, 2004.

[14] EASI, “Facility Electrical Losses: Proximity Effect, Skin Effect, and Eddy Current Losses,” 2015. [Online]. Available: https://www.slideshare.net/abhinaypotlabathini/proximity-effect.

[15] G. Bertotti, “General Properties of Power Losses in Soft Ferromagnetic

Materials.," *IEEE Trans. Magn.*, vol. 24, no. 1, pp. 621–630, 1987.

[16] D. Jiles, "Introduction to Magnetism and Magnetic Materials, " Chapman and Hall. 1991.

[17] R. M. Bozorth, "Ferromagnetic Domains," *Physica*, vol. 1–2, no. September, pp. 207–219, 1949.

[18] R. M. Bozorth, "Ferromagnetism," Wiley-IEEE Press, 1993.

[19] C. D. Graham, B. D. Cullity, "Introduction to Magnetic Materials," 2nd edition, Willey, 2009.

[20] R. J. Bishop, R. E. Smallman, "Modern Physical Metallurgy and Materials Engineering," *Mod. Phys. Metall. Mater. Eng.*, pp. 320–350, 1999.

[21] Hitachi Metals, "MP7438MDGC Data Sheet." .

[22] Metglas, "Material safety data sheet," 2009. [Online]. Available: http://www.metglas.com/assets/pdf/msds/msds2605sa1.pdf.

[23] Metglas, "Amorphous Alloys for Transformer Cores," 2011. [Online]. Available: http://www.metglas.com/assets/pdf/2605sa1.pdf.

[24] Y. Yoshizawa, S. Oguma, and K. Yamauchi, "Fe-Based Soft Magnetic Alloys composed of Ultrafine Grain Structure," *Materials (Basel).*, vol. 31, no. 4, pp. 307–314, 1990.

[25] Hitachi Metals Ltd, "Nanocrystalline Soft Magnetic Material ® Metglass," 2005.

[26] L. Hitachi Metals, "Common Mode Choke Cores," pp. 4–6, 2014.

[27] Magnetics Inc, "Learn More about Powder Cores." [Online]. Available: https://www.mag-inc.com/products/powder-cores/learn-more-about-powder-cores. [Accessed: 23-Apr-2017].

[28] Magnetics Inc, "Powder Core Catalog," 2015. [Online]. Available: https://www.mag-inc.com/getattachment/Design/Design-Guides/2015-Magnetics-Powder-Core-Catalog.pdf?lang=en-US.

[29] Magnetics Inc, "Learn More about Ferrite Cores." [Online]. Available: https://www.mag-inc.com/Products/Ferrite-Cores/Learn-More-about-Ferrite-Cores. [Accessed: 23-Apr-2017].

[30] Magnetics Inc, "F Material." [Online]. Available: https://www.mag-inc.com/Products/Ferrite-Cores/F-Material. [Accessed: 23-Apr-2017].

[31] B. York, "Inductor Design with Continous DC Current." [Online]. Available: http://studylib.net/doc/18253293/toroid-design.

[32] L. R. Diana, "Practical Magnetic Design Inductors and Coupled Inductors." [Online]. Available: https://www.ieee.li/pdf/essay/practical_magnetic_design.pdf.

[33] R. Jez and A. Polit, “Influence of Air Gap Length and Cross-Section on Magnetic Circuit Parameters,” *Excerpt from proceeding 2014 COMSOL Conf. Cambridge*, 2014.

[34] J. Qiu, A. J. Hanson, and C. R. Sullivan, “Design of Toroidal Inductors with Multiple Parallel Foil Windings,” *2013 IEEE 14th Work. Control Model. Power Electron. COMPEL 2013*, pp. 0–5, 2013.

[35] Magnetics Inc, “Ferrite Materials: Ferrite Cores.” [Online]. Available: https://www.mag-inc.com/Products/Ferrite-Cores. [Accessed: 23-Apr-2017].

[36] Magnetics Inc, “C055106A2 Data Sheet,” no. 1. p. 55106, 2014.

[37] Manetics Inc, “0F46113TC Data Sheet,” 2005.

[38] F. M. M. Rahman, “Converter-side Inductor Design for a Grid-connected Converter Equipped with an LCL Filter,” Aalto University School of Electrical Engineering, 2016.

[39] Magnetics, “Ferrite Cores,” 2017. [Online]. Available: https://www.mag-inc.com/getattachment/Products/Ferrite-Cores/Ferrite-Toroids/Learn-More-about-Toroids/Magnetics-Ferrite-Catalog-2017.pdf?lang=en-US.

[40] IEEE Power Electronics Society, “IEEE Standard for Test Procedures for Magnetic Cores IEEE Standard for Test Procedures for Magnetic Cores,” vol. 1991, 1992.

[41] A. Hilal, M. A. Raulet, C. Martin, and F. Sixdenier, “Power loss prediction and Precise Modeling of Magnetic Powder components in DC-DC Power Converter Application,” *IEEE Trans. Power Electron.*, vol. 30, no. 4, pp. 2232–2238, 2015.

[42] Y. H. Y. Han, W. Eberle, and Y.-F. L. Y.-F. Liu, “New measurement Methods to Characterize Transformer Core Loss and Copper Loss in High Frequency Switching Mode Power Supplies,” *2004 IEEE 35th Annu. Power Electron. Spec. Conf. (IEEE Cat. No.04CH37551)*, vol. 2, no. 2, pp. 1695–1701, 2004.